$K\bar{K}$ molecules

John Weinstein
Department of Physics, University of Tennessee, Knoxville, Tennessee 37996-1200

Nathan Isgur
Department of Physics, University of Toronto, Toronto, Ontario, Canada M5S 1A7
(Received 9 May 1989; revised manuscript received 21 February 1990)

We have extended and improved our previous studies of the $qq\bar{q}\,\bar{q}$ system, paying special attention to the $K\bar{K}$ channels. The new results clarify and reinforce the $K\bar{K}$ molecule interpretation of the S^* and δ. Effective meson-meson potentials extracted from the $qq\bar{q}\,\bar{q}$ system and couplings to $q\bar{q}$ scalar mesons lead to coupled-channel amplitudes which closely resemble those observed in both the S^* and δ channels. We also show that the $K\bar{K}$ molecules have properties consisent with experimental results on the production of the S^* and δ and of low-mass $K\bar{K}$ pairs.

I. INTRODUCTION

It now seems unlikely that the $S^*(975)$ and $\delta(980)$ resonances [the $f_0(975)$ and the $a_0(980)$] are simple $q\bar{q}$ mesons. In view of this, and considering the importance of the scalar-meson channel in the search for glueballs, we have continued our studies of the $K\bar{K}$ molecule interpretation of the S^* and δ. In this paper we report new findings which expand, clarify, and reinforce our original results[1] based on a more rudimentary model of the $qq\bar{q}\,\bar{q}$ system.

These two lightest scalar mesons, with $IJ^{PC}=00^{++}$ and 10^{++}, respectively, have a long history of being difficult to accommodate as members of the $1\,^3P_0$ $q\bar{q}$ nonet expected in the 1 to 1.5-GeV mass range.[2] We will discuss extensively the properties of the S^* and δ in Sec. IV, but here we recall some of the difficulties they present to a $q\bar{q}$ interpretation.

(1) Their near degeneracy suggests that they are an almost ideally mixed (ω,ρ)-like doublet. However, if this were the case, then $\Gamma(S^*\to\pi\pi)/\Gamma(\delta\to\eta\pi)$ would be about 4 in contrast with the observed value of about $\frac{1}{2}$ (Refs. 3 and 4).

(2) Both the S^* and δ seem to be very strongly coupled to the $K\bar{K}$ channel: the $\pi\pi$ and $\eta\pi$ mass distributions associated with these states display an otherwise normal Breit-Wigner shape which is dramatically cut off at $K\bar{K}$ threshold. For an (ω,ρ)-like doublet this behavior is unexpected; for example, one would predict that $\Gamma(S^*\to K\bar{K})/\Gamma(S^*\to\pi\pi)\simeq p_K/3p_\pi$.

(3) The observed narrow total widths of the S^* and δ do not fit into otherwise successful models for the decays of the $q\bar{q}$ states. In the pointlike pseudoscalar emission model,[3] the quark-pair-creation model,[4,5] and the flux-tube-breaking model[4] for meson decays, the amplitudes for the decays of the $^3P_0$ $q\bar{q}$ scalars differ from the well-known S-wave part of $b_1(1235)\to\omega\pi$ (b_1 is the $I=1$, $1\,^1P_1$ state) only by some spin and flavor coupling factors. For example, assuming the S^* is a pure ω-like state, these models all predict

$$\frac{\Gamma(S^*\to\pi\pi)}{\Gamma(b_1\to(\omega\pi)S)}=\tfrac{9}{2}\times\text{phase-space-dependent factor},$$

where the "phase-space-dependent factor" would be unity were it not for the different decay momenta of 467 MeV/c and 350 MeV/c, respectively, and which in the models varies between 0.7 and 1.5. Since $\Gamma(b_1\to(\omega\pi)_S)\simeq 150$ MeV, these models thus predict $\Gamma(S^*\to\pi\pi)$ to be between 500 and 1000 MeV, so far from the observed partial width of about 30 MeV that something seems to be seriously wrong. [There is a significant but smaller discrepancy for $\Gamma(\delta\to\eta\pi)$ which has almost exactly the same phase space as $b_1\to\omega\pi$.]

(4) If the S^* and δ are $q\bar{q}$ $1\,^3P_0$ states, then their couplings to $\gamma\gamma$ can be computed in terms of the measured couplings of their SU(6)×O(3) counterparts, the $1\,^3P_2$ states $f_2(1270)$ and $a_2(1320)$. These predictions fail.[6]

(5) Recent studies[7,8] of the reactions $\psi\to VX$ where $V=\rho,\omega,\phi$ is a "flavor-tagging" vector meson and X is a scalar or tensor meson, show once again that the S^* and δ do not behave as analogs of the $f_2(1270)$ and the $a_2(1320)$. For example, $\Gamma(\psi\to\omega S^*)/\Gamma(\psi\to\omega f_2)\lesssim 10^{-2}$, while the S^* is the dominant state seen in $\psi\to\phi\pi^+\pi^-$. Equally anomalous behavior is observed for the δ.

A possible solution to the puzzle presented by these states was suggested by Jaffe on the basis of calculations of the properties of $qq\bar{q}\,\bar{q}$ in the spherical-cavity approximation to the bag model.[9] In these calculations color-magnetic forces stabilized families of $qq\bar{q}\,\bar{q}$ mesons with flavor quantum numbers identical to those of ordinary meson nonets (hence the name "cryptoexotic"). Jaffe pointed out that some of the peculiar properties of the S^* and δ were suggestive of their being two members of the scalar cryptoexotic nonet.

In Refs. 1 we studied the $qq\bar{q}\,\bar{q}$ system in a potential model. One of the biggest advantages of such a calculation over the bag-model calculations is that in the latter approach total confinement is imposed by the boundary condition, while in a potential model the possible binding of the $qq\bar{q}\,\bar{q}$ system is entirely a dynamical question. Our

 ©1990 The American Physical Society

calculation suggested, as did Jaffe's, that the S^* and δ were $qq\bar{q}\,\bar{q}$ states, but of a very different sort: we found that they corresponded to very weakly bound $K\bar{K}$ systems in both the isoscalar and isovector channels. Thus, instead of having four quarks in a single hadron symmetrically arranged about their center of mass, we have two loosely bound mesons. Moreover, instead of finding a complete nonet of scalars, our calculation indicated that only these two bound states should exist. The $K\bar{K}$ molecule interpretation also explained the observed narrowness of the two objects (the bag model predicts a broad δ), and of course it automatically leads to an explanation of why they are both found just below $K\bar{K}$ threshold. The model also provides an understanding of the absence of a rich spectrum of $qq\bar{q}\,\bar{q}$ states, suggesting that such sectors are most appropriately viewed as interacting meson-meson systems.

We will see, in what follows, that the $K\bar{K}$ molecule picture indeed provides a natural interpretation for the observed properties of the S^* and δ. We will also argue that the potential models are a more appropriate method for approaching $qq\bar{q}\,\bar{q}$ dynamics than the naive bag model.[10]

II. THE NEW, IMPROVED CALCULATION

A. The improvements

The calculations of Refs. 1 were exploratory, and as such were based on the simplest model which bore some semblance to reality. Many features of that calculation have now been improved.

(1) References 1 assumed SU(3) symmetry, and in particular that all four quarks have the same mass. This meant that the $qq\bar{q}\,\bar{q}$ system was very symmetric, which enormously simplified the calculations. Unfortunately, this symmetry is not always realistic. We now make no such assumption and so avoid the *ad hoc* prescriptions of Refs. 1 in which this common mass was taken to be the average mass of the four quarks and by which various SU(3)-breaking effects were built in by hand.

(2) References 1 are based on a Hamiltonian in which the only interactions were harmonic confinement and hyperfine interactions. Here the unrealistic but convenient harmonic potential is replaced by a central interaction which is of the standard Coulomb-plus-linear type. The parameters of this Hamiltonian are determined by the spectroscopy of S-, P-, and D-wave mesons, guaranteeing that the basic interquark interactions are accurate in those sectors where they are known.

(3) A corollary of improvement (1) above is that we can now split the $qq\bar{q}\,\bar{q}$ problem up into distinct $(q\bar{q})+(q\bar{q})$ channels with separate thresholds.

B. The Hamiltonian

As our basic Hamiltonian we take

$$H=\sum_{i=1}^{4}\left[m_i+\frac{p_i^2}{2m_i}\right]+H_{\rm SI}+H_{\rm SD}\ , \tag{1}$$

where the spin-independent potential is

$$H_{\rm SI}=-\sum_{i<j}(-\alpha_s\tilde{r}_{ij}^{-1}+\tfrac{3}{4}c+\tfrac{3}{4}br_{ij})\mathbf{F}_i\cdot\mathbf{F}_j \tag{2}$$

and the spin-dependent potential is

$$H_{\rm SD}=-\sum_{i<j}\frac{8\pi\alpha_s}{3m_im_j}\tilde{\delta}^3(r_{ij})\mathbf{S}_i\cdot\mathbf{S}_j\mathbf{F}_i\cdot\mathbf{F}_j+H_{\rm ten}+H_{\rm SO}\ , \tag{3}$$

where

$$\mathbf{F}_i=\begin{cases}\dfrac{\lambda_i}{2} & \text{for a quark}\ ,\\ -\dfrac{\lambda_i^*}{2} & \text{for an antiquark}\ ,\end{cases} \tag{4}$$

is the color matrix, and m_i, $\mathbf{r}_i$, $\mathbf{p}_i$, and $\mathbf{S}_i$ are the mass, position, momentum, and spin of the ith particle, and $\tilde{\delta}^3(\mathbf{r})$ and $\tilde{r}^{-1}$ are smeared versions of the operators $\delta^3(\mathbf{r})$ and r^{-1}. (These modified operators partially account for relativistic corrections; they are described in Appendix A.) We do not specify the tensor and spin-orbit interactions $H_{\rm ten}$ and $H_{\rm SO}$ in (3) because we ignore them in what follows; they are small and for the dominantly S-wave ground states which are the objects of this study, they would have little effect in any event. As already mentioned, the parameters of the Hamiltonian are determined by a fit to the $1S$, $1P$, and $1D$ states of ordinary meson spectroscopy. This fit gives $m_u=m_d=0.375$ GeV, $m_s=0.600$ GeV, $c=-1.036$ GeV, $b=0.178$ GeV^2, and $\alpha_s=0.748$.

While this Hamiltonian is now a much more realistic representation of the physics of the $qq\bar{q}\,\bar{q}$ system than that of Refs. 1, it is not without many of the same problems. Among these are the following.

(1) $\mathbf{F}_i\cdot\mathbf{F}_j$ confinement. In our model for $H_{\rm SI}$, $H_{\rm SI}^{ij}$ is proportional to $\mathbf{F}_i\cdot\mathbf{F}_j$ (Ref. 11). This model is known to be flawed phenomenologically because it leads to power-law van der Waals' forces between color-singlet hadrons.[1,11] It is also flawed theoretically in that it is very implausible that the long-range static $qq\bar{q}\,\bar{q}$ potential is just a sum of the two-body potentials. (This problem is related to the fact that this model does not respect local color gauge invariance.[11]) Despite these defects we believe that the use of the model is justifiable. It was already argued in Refs. 1 that the $\mathbf{F}_i\cdot\mathbf{F}_j$ model has many desirable characteristics. For example, if any physical (i.e., color-singlet) multiquark system is divided into two color clusters C and $\bar{C}$, the model automatically confines them with a string tension proportional to the appropriate $\mathrm{SU}(3)_C$ Casimir constant. The model also allows the asymptotic separation of a multiquark system into noninteracting color-singlet clusters, and it leads to potentials in mesonlike $q\bar{q}$ and baryonlike qqq subsystems in accord with the empirically known potentials. Despite all of these satisfactory properties, it was not possible in Refs. 1 to justify (or check empirically) other properties of the model, in particular its crucial predictions for matrix elements which involve color transitions (such as

$1_{13}1_{24} \leftrightarrow 8_{13}8_{24}$; see below) within clusters. Since the publication of Refs. 1, the status of the $\mathbf{F}_i \cdot \mathbf{F}_j$ model as a legitimate representation of confinement has become much clearer through the work of Ref. 12 on the flux-tube model of confinement. This latter model, which has explicit local color gauge invariance, is based on the strong-coupling limit of Hamiltonian lattice QCD. In this model one can see that the two-dimensional color basis of the $\mathbf{F}_i \cdot \mathbf{F}_j$ model (see Sec. III below for details) is a truncation of the complete flux-tube basis. However, one can also see that the truncation is a good one in the sense that it closely reproduces the two lowest-lying adiabatic potentials of the flux-tube model. In particular, the $\mathbf{F}_i \cdot \mathbf{F}_j$ model qualitatively reproduces the expected color mixing effects. It fails quantitatively in predicting the rapid decrease of color mixing for increasing meson-meson separation (which leads to the rapid decrease of van der Waals' forces) because it is a truncation, but we view this as a minor flaw with effects that can for the most part be readily compensated. This will be particularly true for the system at hand: as emphasized in Refs. 13, its structure is dominated by the better understood short-range forces.

(2) Nonrelativistic dynamics. A persistent problem of the quark potential model is the assessment of the importance of relativistic effects. In the cases of mesons and baryons there is now considerable evidence to support the view that the hadrons are relativistic (as opposed to ultrarelativistic) systems which can be studied by extrapolation from the nonrelativistic limit. [That is, for the light quarks both m and p are of the order of $\Lambda_{\rm QCD}$. Thus p/m is of order unity (not infinity) so that the basic structure of such systems is similar to that of the nonrelativistic limit.] Nevertheless, in each particular case one must carefully analyze the reliability of results based on the nonrelativistic framework. In a very large number of situations one can argue that the main effects of relativistic corrections have been absorbed into the effective nonrelativistic parameters [e.g., the quark masses and the string tension hide the difference between the energies $(p^2+m^2)^{1/2}$ and $(m+p^2/2m)$]. In the case at hand, there is, however, one particularly severe problem with the nonrelativistic framework that has strongly influenced our approach. Consider a configuration of $q_1q_2\bar{q}_3\bar{q}_4$ corresponding to two interacting color-singlet mesons $(q_1\bar{q}_3)_1$ and $(q_2\bar{q}_4)_1$. The nonrelativistic framework will produce kinetic energy operators for these two clusters in which their masses are (m_1+m_3) and (m_2+m_4), independent of their internal interactions (i.e., nonrelativistically the mass of a system is always the sum of its constituent masses). We will address this defect by adopting methods designed to freeze out the cluster kinetic energies, extract effective meson-meson potentials, and then solve the (coupled channel) Schrödinger equation with the correct physical masses of the $q\bar{q}$ clusters using these effective potentials.

(3) The treatment of $q\bar{q}$ annihilation. Our potential model is suited to studying the effects of ordinary potentials on the $qq\bar{q}\,\bar{q}$ system. However, there are additional annihilation reactions that can occur when a quark and antiquark of the same flavor appear in the $qq\bar{q}\,\bar{q}$ system. The three types of annihilation which can occur are shown in Fig. 1. The effects of Fig. 1(a), annihilation into an ordinary meson, are easily added to the potential model and are discussed below. The effects of Fig. 1(b), annihilation into a hybrid meson[12,14,15] (i.e., a $q\bar{q}$ state with excited glue) could also easily be included. There are, however, both experimental and theoretical grounds for believing that the lightest such states will have masses of about 2 GeV, well above the $K\bar{K}$ threshold region which we are investigating. We therefore simply ignore the effects of these states. Unlike the first two cases, annihilation via Fig. 1(c), in which the intermediate state consists of an ordinary $q\bar{q}$ meson remnant of the original $qq\bar{q}\,\bar{q}$ state along with a (virtual) glueball,[16] turns out to be problematical since $q\bar{q}$ annihilation is very strong in the pseudoscalar-meson sector which will play a central role in what follows. Without this process we would have an η with quark content $(1/\sqrt{2})(u\bar{u}+d\bar{d})$ and the mass of the pion and a pure $s\bar{s}$ η' (Ref. 17). As we will find that the $qq\bar{q}\,\bar{q}$ system is well approximated as a system of interacting mesons, it is probable that the main effect of this interaction in $qq\bar{q}\,\bar{q}$ is to nearly recreate within its $q\bar{q}$ clusters the free meson eigenstates. We will accordingly assume that the annihilation of Fig. 1(c) simply produces η and η' clusters identical to the free eigenstates (which we approximate by the "perfect mixing" pattern

$$\eta=(1/\sqrt{2})[(1/\sqrt{2})(u\bar{u}+d\bar{d})-s\bar{s}]$$
$$=(1/\sqrt{2})(\eta_{ns}-\eta_{s\bar{s}})\,, \tag{5}$$

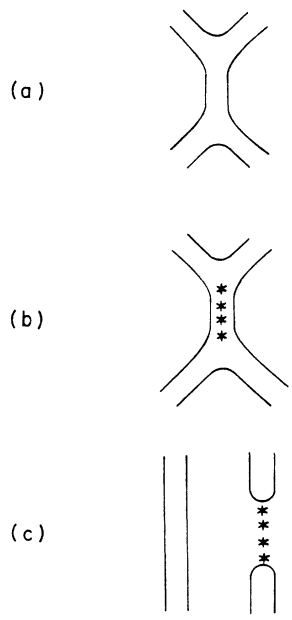

FIG. 1. The three types of $q\bar{q}$ annihilation which can affect the $qq\bar{q}\,\bar{q}$ system: (a) annihilation without gluonic excitation into an ordinary $q\bar{q}$ meson, (b) annihilation with gluonic excitation into a hybrid meson, (c) annihilation in a color singlet $q\bar{q}$ subsystem to produce a (virtual) glueball and an ordinary meson; in these diagrams an asterisk represents excited glue.

$$\eta' = (1/\sqrt{2})[(1/\sqrt{2})(u\bar{u}+d\bar{d})+s\bar{s}]$$
$$= (1/\sqrt{2})(\eta_{ns}+\eta_{s\bar{s}}) , \quad (6)$$

of Ref. 17), and that the effective meson-meson potentials (to be defined precisely below) involving η and η' are the averages over their compositions. Thus, for example,

$$V_{\pi\eta} \equiv \langle \pi\eta | V | \pi\eta \rangle \quad (7)$$
$$= \left\langle \pi \frac{1}{\sqrt{2}}(\eta_{ns}-\eta_{s\bar{s}}) \middle| V \middle| \pi \frac{1}{\sqrt{2}}(\eta_{ns}-\eta_{s\bar{s}}) \right\rangle \quad (8)$$
$$= \tfrac{1}{2}(V_{\pi\eta_{ns}} + V_{\pi\eta_{s\bar{s}}}) \quad (9)$$

and

$$V_{\eta\eta} = V_{\eta\eta'} = V_{\eta'\eta'} = \tfrac{1}{4}(V_{\eta_{ns}\eta_{ns}} + 2V_{\eta_{ns}\eta_{s\bar{s}}} + V_{\eta_{s\bar{s}}\eta_{s\bar{s}}}) . \quad (10)$$

C. Methods

We now describe in some detail the methods we used to extract physics from this model. The first step is to find the four-quark wave function. The most general case of interest here is the one shown in Fig. 2 in which 1 and 2 are quarks and 3 and 4 are antiquarks with masses $m_1 = m_4 = m$ and $m_2 = m_3 = m'$. [Thus (1,3) and (2,4) will be associated with the K and $\bar{K}$, respectively.] In this case an obvious set of coordinates is

$$\mathbf{r}_{13} \equiv \mathbf{r}_1 - \mathbf{r}_3 , \quad (11)$$

$$\mathbf{r}_{24} \equiv \mathbf{r}_2 - \mathbf{r}_4 , \quad (12)$$

$$\mathbf{x}' \equiv \left[\frac{m\mathbf{r}_1 + m'\mathbf{r}_3}{m+m'}\right] - \left[\frac{m'\mathbf{r}_2 + m\mathbf{r}_4}{m+m'}\right]$$
$$= \frac{m(\mathbf{r}_1-\mathbf{r}_4) + m'(\mathbf{r}_3-\mathbf{r}_2)}{m+m'} , \quad (13)$$

$$\mathbf{R}_{\text{c.m.}} \equiv \frac{m(\mathbf{r}_1+\mathbf{r}_4) + m'(\mathbf{r}_2+\mathbf{r}_3)}{2(m+m')} , \quad (14)$$

in terms of which the four-quark kinetic energy is simply

$$H_0 = \frac{P^2_{\text{c.m.}}}{2M} + \frac{P^2_{13}+P^2_{24}}{2\mu} + \frac{P^2_{x'}}{2\mu_{x'}} \quad (15)$$

with $M = 2(m+m')$, $\mu = mm'/(m+m')$, and $\mu_{x'} = \frac{1}{2}(m+m')$. However, much of this calculation involves the evaluation of matrix elements of functions of the interquark distances, and for these purposes it is convenient to use the symmetric relative coordinates

$$\mathbf{x} = \tfrac{1}{2}(\mathbf{r}_1 - \mathbf{r}_2 + \mathbf{r}_3 - \mathbf{r}_4) , \quad (16)$$

$$\mathbf{a} = \tfrac{1}{2}(\mathbf{r}_1 + \mathbf{r}_2 - \mathbf{r}_3 - \mathbf{r}_4) , \quad (17)$$

$$\mathbf{y} = \tfrac{1}{2}(\mathbf{r}_1 - \mathbf{r}_2 - \mathbf{r}_3 + \mathbf{r}_4) , \quad (18)$$

used in Refs. 1. With this choice the kinetic energy operator becomes

$$H_0 = \frac{P^2_{\text{c.m.}}}{2M} + \frac{P_x^2+P_a^2+P_y^2}{4\mu} + \left[\frac{m'-m}{m'+m}\right]\frac{\mathbf{P}_x\cdot\mathbf{P}_a}{2\mu} ; \quad (19)$$

note that for S waves the matrix elements of the last term vanish.

With its three relative coordinates and nontrivial color, spin, and space couplings, the $qq\bar{q}\,\bar{q}$ system is a very complicated one that poses formidable obstacles to a comprehensive solution. (We note that even the toy problem[18] in which the *only* interaction is $-\sum_{i<j}\frac{1}{2}kr_{ij}^2\mathbf{F}_i\cdot\mathbf{F}_j$ remains unsolved. A solution would be very interesting for the light it might shed on the problem of high angular momentum baryonium.[19]) Here, however, our goals are much more modest and allow us to adopt a calculationally tractable (though convoluted) strategy.

(a) We solve variationally for the ground state of the $qq\bar{q}\,\bar{q}$ system. We do this calculation in a large "box" (by methods to be described below) so that even if the ground state of the system naturally corresponds to two free mesons, their interactions can still be studied.

(b) Out of the full ground-state $qq\bar{q}\,\bar{q}$ wave function we project amplitudes $\psi_A(\mathbf{r})$ to find a system A of mesons (e.g., $A = K\bar{K}$) at relative separation $\mathbf{r}$. This is done using our calculated $q\bar{q}$ wave functions for the mesons in A as detailed below. This decomposition is most useful when the full $qq\bar{q}\,\bar{q}$ wave function corresponds to two weakly bound or unbound mesons, which is always the case for the systems we study here.

(c) Having (partially) decomposed the complicated $qq\bar{q}\,\bar{q}$ wave function into a set of wave functions $\psi_A(\mathbf{r})$, $\psi_B(\mathbf{r}), \ldots$, we then map our problem onto the multichannel scattering problem

$$H_{ij}\psi_j = \left[\left(M_i + \frac{p^2}{2\mu_i} + V_i\right)\delta_{ij} + W_{ij}\right]\psi_j = E\psi_i \quad (20)$$

in which $i = A, B, \ldots, M_i$ is the sum of the meson masses in the ith channel, μ_i is the [nonrelativistically determined: see Eq. (15)] reduced mass of the two mesons of the ith channel, V_i is their effective potential, and $W_{ij} = W_{ij}^* = W_{ji}$ is the transition potential from channel i to j. Since the N channel problem is characterized by $\frac{1}{2}N(N+1)$ potentials, it is clear (since $N>1$) that the N extracted ground-state wave functions are insufficient to determine them. However, we could obtain a set of such wave functions for every size "box" we choose, and hence in principle sufficient information to make this mapping. In practice it turns out to be difficult to determine the wave functions with sufficient accuracy to use this method, and so we use instead (approximate) excited states of the $qq\bar{q}\,\bar{q}$ system in a fixed box. We will give the

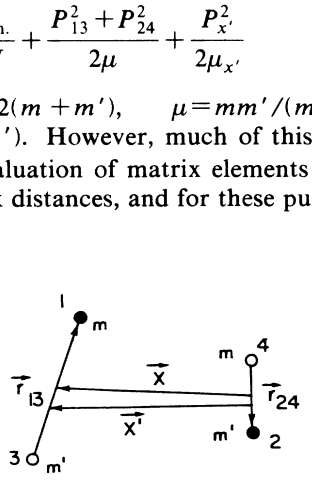

FIG. 2. The $qq\bar{q}\,\bar{q}$ system, showing the labeling of the particles and their relative coordinates.

details of this procedure below.

(d) The off-diagonal potentials W_{ij} obtained in this way all correspond to possible quark exchange (i.e., rearrangement) reactions in the $qq\bar{q}\,\bar{q}$ system, e.g., $K\bar{K}\leftrightarrow\eta\pi$. In some cases, however, there are important channel couplings which cannot proceed in this way. The most significant for us is the coupling $K\bar{K}\leftrightarrow\pi\pi$ which requires quark annihilation, and so is not present in this potential-model calculation. Such couplings arise via the processes of Fig. 1, either in higher order through, e.g., $K\bar{K}\rightarrow\eta\eta\rightarrow\pi\pi$ using Fig. 1(c) or directly through the broad $1\,^3P_0$ $q\bar{q}$ scalar mesons[3] as shown in Fig. 1(a). As explained in Appendix B, the coupling between the $qq\bar{q}\,\bar{q}$ and $q\bar{q}$ sectors [to take into account Fig. 1(a)] is built into our system by adding (closed) $q\bar{q}$ channels to the coupled-channel equations (20). The coupling potentials Ω_{ij} between meson-meson and $q\bar{q}$ channels are chosen to reproduce the predicted couplings of the flux-tube-breaking[4] (or $^3P_0$, Refs. 4 and 5) model.

(e) With the very complex $qq\bar{q}\,\bar{q}$ system now modeled by a "simple" coupled-channel problem with effective potentials, we solve, with the *correct* physical masses of the mesons, for the appropriate transition matrix elements and compare with experiment. The advantage of these procedures, aside from their sidestepping some of the inadequacies of our nonrelativistic model, is that they have allowed us to convert our knowledge of the ground-state wave functions of the $qq\bar{q}\,\bar{q}$ and $q\bar{q}$ systems into information about the behavior of meson-meson scattering as a function of energy.

III. THE CALCULATIONS

A. Variational solution

Our calculation is based on solving variationally for the ground state of the $qq\bar{q}\,\bar{q}$ system with the Hamiltonian (1) and so requires an adequate variational wave function. The general $qq\bar{q}\,\bar{q}$ wave function is very rich in structure even in our simplified model. There is, first of all, a two-dimensional color space. One could use any of the orthonormal pairs $(|\bar{3}_{12}3_{34}\rangle, |6_{12}\bar{6}_{34}\rangle)$, $(|1_{13}1_{24}\rangle, |8_{13}8_{24}\rangle)$, or $(|1_{14}1_{23}\rangle, |8_{14}8_{23}\rangle)$ as a basis for this space. (Here $|C_{ij}\bar{C}_{kl}\rangle$ indicates that cluster ij is in the color state C, kl is in $\bar{C}$, and that the whole system is coupled to a color singlet. These bases, and the relations between them, are given in Appendix C.) Alternatively (and this is the choice we made) one could use a complete but nonorthogonal basis such as $(|1_{13}1_{24}\rangle, |1_{14}1_{23}\rangle)$ which corresponds more directly to the allowed asymptotic color states of the Hamiltonian. The system also has a multidimensional spin space: $\frac{1}{2}\otimes\frac{1}{2}\otimes\frac{1}{2}\otimes\frac{1}{2}=2\oplus1\oplus1\oplus1\oplus0\oplus0$. Since we are interested in the ground state of the $J^P=0^+$ sector of this system, we naturally focus on the two-dimensional subspace of spin zero (various spin bases and their relationships are given in Appendix D). In fact, with our previously mentioned neglect of tensor and spin-orbit forces, the Hamiltonian separately conserves **L** and **S**, so we can restrict our considerations to this $S=0$ sector, which in turn means we will be dealing only with $L=0$ spatial wave functions.

We have not yet discussed the $qq\bar{q}\,\bar{q}$ flavor wave function. If the two quarks (or the two antiquarks) have the same flavor then only color-spin-space wave functions which are antisymmetric under their interchange will be allowed. In our case, we are only peripherally interested in this possibility: the $K\bar{K}$ systems on which we focus have quark contents $us\,\bar{u}\,\bar{s}$, $us\,\bar{d}\,\bar{s}$, $ds\,\bar{d}\,\bar{s}$, and $ds\,\bar{u}\,\bar{s}$ so that the Pauli exclusion principle never applies. On the other hand we will consider systems such as $\pi\pi$ and $\eta\eta$ where it does apply. In addition, we will find it very important to be able to refer to the SU(3) limit where $m_u=m_d=m_s$. In that case the Hamiltonian is separately $1\leftrightarrow2$ and $3\leftrightarrow4$ symmetric which means that its eigenfunctions can be classified as being either Fermi or Bose under these separate interchanges in the color-spin-space wave functions. Since the SU(3)-symmetric Hamiltonian is also invariant under the simultaneous interchange $P_{13}P_{24}$ of quarks and antiquarks, one can show that the $J^{PC_n}=0^{++}$ wave functions are in fact either "doubly Bose" or "doubly Fermi" giving an SU(3)-flavor structure that is $|\bar{3}_{12}3_{24}\rangle$ and $|6_{12}\bar{6}_{34}\rangle$, respectively. The former nine flavor states comprise a cryptoexotic nonet;[9] the latter states can produce systems with exotic flavor quantum numbers.

This brings us finally to the spatial wave functions $\psi_\alpha(\mathbf{x},\mathbf{a},\mathbf{y})$ multiplying a given color-spin wave function associated with the index α. As shown in Refs. 1, this function must be an eigenstate of each of $\mathbf{L}_x$, $\mathbf{L}_a$, and $\mathbf{L}_y$ in the harmonic limit with $m=m'$ so that the ground-state wave function with $l_x=l_a=l_y=0$ will depend only on x^2, a^2, and y^2. In the case at hand the anharmonicities in the true potential and SU(3) breaking will induce dependence on $\mathbf{x}\cdot\mathbf{a}$, $\mathbf{x}\cdot\mathbf{y}$, and $\mathbf{a}\cdot\mathbf{y}$. However, one can show that, in a perturbative expansion, such terms will first enter the wave function as fourth-order polynomials of the form $(\mathbf{x}\cdot\mathbf{y})^2$ and $\frac{1}{2}[(\mathbf{x}\cdot\mathbf{a})^2+(\mathbf{y}\cdot\mathbf{a})^2]$. Since such fourth-order excitations of the harmonic system are very high in mass, we expect their contribution to be small. Indeed, our explicit attempts to include such terms led to negligible effects. We accordingly performed almost all of our calculations in the relatively simple variational space spanned by the wave function (used already in Ref. 1)

$$\psi_\alpha(\mathbf{x},\mathbf{a},\mathbf{y})=\sum_{j=1}^{j_{\max}}\prod_{i=1}^{3}\sum_{k=1}^{k_{\max}} C_{\alpha ijk}\exp(-\tfrac{1}{2}\beta_{\alpha ijk}^2\xi_i^2)\ , \qquad (21)$$

where $(\xi_1,\xi_2,\xi_3)\equiv(\mathbf{x},\mathbf{a},\mathbf{y})$ and the C's and β's are our variational parameters. The largest wave function we considered had $j_{\max}=2$ and $k_{\max}=4$, corresponding to a 44-parameter wave function for each index α. Of course this wave function is still incomplete but, as will be made clear below, the fact that we thereby underestimate the binding of the $K\bar{K}$ system will strengthen our main conclusions.

Given the assumptions we have already made, the state vector of the $qq\bar{q}\,\bar{q}$ system is restricted to be of the form

$$|\psi\rangle=\sum_\alpha \psi_\alpha(\mathbf{x},\mathbf{a},\mathbf{y})|\alpha\rangle\ , \qquad (22)$$

where the four-dimensional color-spin basis α may be

taken to be either the basis with explicit $1\leftrightarrow 2$ and $3\leftrightarrow 4$ symmetry, namely (see Appendixes C and D for definitions), $|\bar{3}_{12}3_{24}\rangle|S_{12}S_{34}\rangle$, $|\bar{3}_{12}3_{34}\rangle|\mathbf{A}_{12}\cdot\mathbf{A}_{34}\rangle$, $|6_{12}\bar{6}_{34}\rangle|S_{12}S_{34}\rangle$, and $|6_{12}\bar{6}_{34}\rangle|\mathbf{A}_{12}\cdot\mathbf{A}_{34}\rangle$, the "physical basis" which we use,

$$|1\rangle=|1_{13}1_{24}\rangle|P_{13}P_{24}\rangle\ , \tag{23a}$$

$$|2\rangle=|1_{14}1_{23}\rangle|P_{14}P_{23}\rangle\ , \tag{23b}$$

$$|3\rangle=|1_{13}1_{24}\rangle|\mathbf{V}_{13}\cdot\mathbf{V}_{24}\rangle\ , \tag{24a}$$

$$|4\rangle=|1_{14}1_{23}\rangle|\mathbf{V}_{14}\cdot\mathbf{V}_{23}\rangle\ , \tag{24b}$$

or any other complete set. Our use of the "physical basis" is motivated by the fact that if the $qq\bar{q}\,\bar{q}$ system is unbound, its ground states will be proportional to the states (23) and (24) which have the correct color-spin structure to represent two free pseudoscalar or two free vector mesons.

With the form of the variational wave function decided, the real work begins: computing the matrix elements of the Hamiltonian with the state (22). These calculations are tedious, but straightforward, so we do not discuss them here. Some useful matrix elements for the calculation are given in Appendixes C and D.

The search for the ground-state wave function in the very large space spanned by (22) is, in many cases, only feasible when we add a weak color-independent harmonic confinement potential $H_\epsilon=\sum_{i<j}\frac{1}{2}\epsilon r_{ij}^2$ to the Hamiltonian (1). This "harmonic box" localizes the $qq\bar{q}\,\bar{q}$ system so that the variational wave function can respond to an attractive (but nonbinding) or repulsive potential. The effect of H_ϵ can then be subtracted from the deduced effective potential corresponding to the channel α. H_ϵ also removes an inevitable but spurious effective potential found at large r when one uses harmonic variational wave functions. We have checked that this procedure works in a simple two-body problem by starting with a known potential, adding H_ϵ, finding the variational wave function, and then extracting from it the input potential by the analog of the technique of the next subsection. Incidentally, we find that the low-energy phase shifts deduced from these effective potentials converges under expansion of our variational space much more quickly than the potentials themselves.

B. Effective potentials

From the full $qq\bar{q}\,\bar{q}$ wave function of Eq. (22) we next project a set of (ground-state) meson-meson scattering channels corresponding to the effective Hamiltonian of Eq. (20). Thus we define

$$\psi_1(\mathbf{r})\equiv 2^{3/2}\int\int d^3a\,d^3y\,\psi_{13}^*(\mathbf{a}+\mathbf{y})\psi_{24}^*(\mathbf{a}-\mathbf{y})\times\psi_1(\mathbf{r},\mathbf{a},\mathbf{y})\ , \tag{25a}$$

$$\psi_2(\mathbf{r})\equiv 2^{3/2}\int\int d^3a\,d^3y\,\psi_{14}^*(\mathbf{a}+\mathbf{x})\psi_{23}^*(\mathbf{a}-\mathbf{x})\times\psi_2(\mathbf{x},\mathbf{a},\mathbf{r})\ , \tag{25b}$$

etc., where $\psi_{ij}(\mathbf{r}_{ij})$ is the ground-state wave function of the appropriate isolated $q_i\bar{q}_j$ meson. We find that the $qq\bar{q}\,\bar{q}$ ground state is totally dominated by the pseudoscalar-pseudoscalar ground states of Eqs. (23).

This basic conclusion concerning the particle content of the 0^{++} $qq\bar{q}\,\bar{q}$ sector is different from that of the bag model, but not as different as it might appear. After correcting for a sign error[13,20] in the [1]–[405] mixing amplitude of Ref. 9, the states of the lowest-lying $qq\bar{q}\,\bar{q}$ scalar nonet have the composition (see Appendixes C and D for notation)

$$|9,0^+\rangle=0.812|6_{12}\bar{6}_{34}\rangle|\mathbf{A}_{12}\cdot\mathbf{A}_{34}\rangle+0.583|\bar{3}_{12}3_{34}\rangle|S_{12}S_{34}\rangle \tag{26}$$

which can be written in terms of the nonorthogonal basis of Eqs. (23) and (24) as

$$|9,0^+\rangle=1.043|PP\rangle_c+0.244|VV\rangle_c\ , \tag{27}$$

where

$$|PP\rangle_c=\sqrt{3/7}(|1\rangle+|2\rangle)\ , \tag{28a}$$

$$|VV\rangle_c=\sqrt{3/5}(|3\rangle+|4\rangle)\ , \tag{28b}$$

are the normalized cryptoexotic color-spin combinations of two pseudoscalars and two vectors. This shows that even in the bag model, where $|PP\rangle_c$ and $|VV\rangle_c$ are being forced to interact by the boundary condition, the lowest-lying scalar nonet is tending toward the pseudoscalar-pseudoscalar composition we find.

In view of the PP dominance of our wave function, it suffices to map our problem onto the multichannel problem of S-wave pseudoscalar-meson–pseudoscalar-meson scattering with a Hamiltonian of the form of Eq. (20) and with the five $I=0$ channels $1\equiv\pi\pi$, $2\equiv K\bar{K}$, $3\equiv\eta\eta$, $4\equiv\eta\eta'$, and $5\equiv\eta'\eta'$, the three $I=1$ channels $1\equiv\pi\eta$, $2\equiv K\bar{K}$, and $3\equiv\pi\eta'$, and the single $I=2$ $\pi\pi$ channel. To carry out this mapping we first consider the SU(3) limit in which the $qq\bar{q}\,\bar{q}$ system's solutions are segregated by symmetry into noncommunicating cryptoexotic and exotic sectors, corresponding in the two-channel approximation to Eq. (20) to the solution spaces $\psi_2=\psi_1$ and $\psi_2=-\psi_1$ which occur when $V_1=V_2\equiv V$. In this case (with $W\equiv W_{12}$) the equations for $\alpha=1,2$ [see Eq. (23)] separate into

$$(M+K+V\pm W)\psi_\pm=E\psi_\pm\ , \tag{29}$$

where $K\equiv\nabla^2/2\mu$ and $\psi_\pm=\psi_1\pm\psi_2$. The cryptoexotic solutions (denoted ψ^c) of these coupled equations then have $\psi^c_+\neq 0$ and $\psi^c_-=0$. In the exotic sector (denoted ψ^e) it is ψ^e_+ that is trivial, and $\psi^e_-\neq 0$. We then have, solving Eq. (29) for $V\pm W$,

$$V^c\equiv V+W=(\psi^c_+)^{-1}(E^c-M-K)\psi^c_+\ , \tag{30}$$

$$V^e\equiv V-W=(\psi^e_-)^{-1}(E^e-M-K)\psi^e_-\ , \tag{31}$$

which yield $V=\frac{1}{2}(V^c+V^e)$ and $W=\frac{1}{2}(V^c-V^e)$. Here E^c and E^e are the cryptoexotic and exotic energy eigenvalues. In terms of this V and W and Table I one can then construct any required potential by using the fact that the scattering will be diagonal in the R,I,I_3,x quantum numbers of Table I, with potentials V^x that depend only on the flavor structure (exoticity) x. One finds

TABLE I. The SU(3) decomposition of various two-pseudoscalar-meson states with $J^{PC}=0^{++}$; $|R,I,I_3,x\rangle$ specifies the SU(3) representation $R=\mathbf{1},\mathbf{8},\mathbf{27}$, isospin I,I_3, and exoticity $x=c$ (cryptoexotic) or e (exotic), and $[A,B]_+\equiv\sqrt{1/2}(AB+BA)$.

	Cryptoexotics			Exotics					
Meson-meson	$\|1,0,0,c\rangle$	$\|8,1,I_3,c\rangle$	$\|8,0,0,c\rangle$	$\|1,0,0,e\rangle$	$\|8,1,I_3,e\rangle$	$\|8,0,0,e\rangle$	$\|27,2,I_3,e\rangle$	$\|27,1,I_3,e\rangle$	$\|27,0,0,e\rangle$
$(\pi\pi)^{I=2}$	0	0	0	0	0	0	1	0	0
$(\pi\pi)^{I=0}$	$1/2$	0	$-\sqrt{1/2}$	$-\sqrt{1/8}$	0	$-\sqrt{1/10}$	0	0	$-\sqrt{1/40}$
$\eta_{ns}\eta_{ns}$	$\sqrt{1/12}$	0	$-\sqrt{1/6}$	$\sqrt{3/8}$	0	$\sqrt{3/10}$	0	0	$\sqrt{3/40}$
$\eta_{s\bar{s}}\eta_{s\bar{s}}$	0	0	0	$\sqrt{1/6}$	0	$-\sqrt{8/15}$	0	0	$\sqrt{3/10}$
$[\eta_{ns}\eta_{s\bar{s}}]_+$	$\sqrt{1/3}$	0	$\sqrt{1/6}$	$\sqrt{1/6}$	0	$-\sqrt{1/30}$	0	0	$-\sqrt{3/10}$
$[\pi\eta_{ns}]_+$	0	0	0	0	$-\sqrt{4/5}$	0	0	$-\sqrt{1/5}$	0
$[\pi\eta_{s\bar{s}}]_+$	0	$-\sqrt{1/2}$	0	0	$-\sqrt{1/10}$	0	0	$+\sqrt{2/5}$	0
$[K\bar{K}^{I=0}]_+$	$\sqrt{1/3}$	0	$\sqrt{1/6}$	$-\sqrt{1/6}$	0	$\sqrt{1/30}$	0	0	$\sqrt{3/10}$
$[K\bar{K}^{I=1}]_+$	0	$-\sqrt{1/2}$	0	0	$\sqrt{1/10}$	0	0	$-\sqrt{2/5}$	0

$$(V+W)^{(I=0)}_{SU(3)}=\begin{bmatrix} V_u+\frac{1}{2}W_u & 0 & \sqrt{3/16}\,W_u & \sqrt{3/16}\,W_u & \sqrt{3/16}\,W_u \\ 0 & V_k & -\sqrt{1/2}\,W_k & 0 & \sqrt{1/2}\,W_k \\ \sqrt{3/16}\,W_u & -\sqrt{1/2}\,W_k & V_{\eta\eta} & W_{\eta\eta;\eta'\eta} & W_{\eta\eta;\eta'\eta'} \\ \sqrt{3/16}\,W_u & 0 & W_{\eta'\eta;\eta\eta} & V_{\eta'\eta} & W_{\eta'\eta;\eta'\eta'} \\ \sqrt{3/16}\,W_u & \sqrt{1/2}\,W_k & W_{\eta'\eta';\eta\eta} & W_{\eta'\eta';\eta'\eta} & V_{\eta'\eta'} \end{bmatrix}, \tag{32}$$

where

$$V_{\eta\eta}=V_{\eta'\eta}=V_{\eta'\eta'}=\tfrac{1}{4}(V_u-\tfrac{1}{2}W_u+2V_k+V_s-W_s),\quad W_{\eta\eta;\eta'\eta}=W_{\eta'\eta';\eta'\eta}=\tfrac{1}{4}(V_u-\tfrac{1}{2}W_u-V_s+W_s),$$

$$W_{\eta\eta;\eta'\eta'}=\tfrac{1}{4}(V_u-\tfrac{1}{2}W_u-2V_k+V_s-W_s),$$

$$(V+W)^{(I=1)}_{SU(3)}=\begin{bmatrix} \frac{1}{2}(V_u+V_k-W_u) & -\sqrt{1/2}\,W_k & \frac{1}{2}(V_u-V_k-W_u) \\ -\sqrt{1/2}\,W_k & V_k & \sqrt{1/2}W_k \\ \frac{1}{2}(V_u-V_k-W_u) & \sqrt{1/2}\,W_k & \frac{1}{2}(V_u+V_k-W_u) \end{bmatrix}, \tag{33}$$

and

$$(V+W)^{(I=2)}_{SU(3)}=V_u-W_u\ . \tag{34}$$

In Eqs. (32)–(34) the direct and exchange potentials V_m and W_m carry a subscript which denotes the average mass of the participating quarks: u for systems with all light (up and down) quarks, k for systems with two light quarks and two strange quarks, and s for systems of four strange quarks. The six extracted potentials are shown in Fig. 3. The use of three "SU(3) limits" with three different values for the average quark mass would, of course, already take into account the most elementary form of SU(3) breaking. As we will now discuss, this simple SU(3)-breaking effect seems to be the dominant one.

With the "SU(3)" potentials V_m and W_m in hand, we return to the $qq\bar{q}\,\bar{q}$ problem with unequal masses in the $\alpha=1,2$ basis, and rewrite Eq. (20):

$$\begin{bmatrix} M_1+K_1+V_1 & W_{12} \\ W_{12} & M_2+K_2+V_2 \end{bmatrix}\begin{bmatrix}\psi_1\\ \psi_2\end{bmatrix}=E\begin{bmatrix}\psi_1\\ \psi_2\end{bmatrix}. \tag{35}$$

We now assume that $W_{12}\approx W_m$ which leads to

$$V_1\simeq\frac{(E-M_1-K_1)\psi_1-W_m\psi_2}{\psi_1} \tag{36}$$

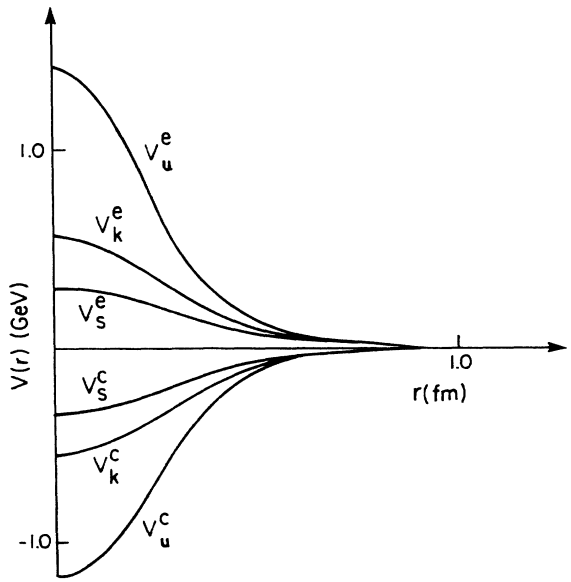

FIG. 3. The six "elementary" extracted potentials V_m^x, $x=c$ for cryptoexotic or e for exotic, $m=u$, k, or s; from these potentials one can deduce $V_m\equiv\frac{1}{2}(V^c+V^e)$ and $W_m\equiv\frac{1}{2}(V^c-V^e)$.

and

$$V_2 \simeq \frac{(E-M_2-K_2)\psi_2 - W_m\psi_1}{\psi_2} . \quad (37)$$

A remark about this approximation is in order. This technique for extracting the SU(3)-broken potentials uses the average mass transition potential W_m rather than W_{12} and forces the residual SU(3) breaking into V_1 and V_2. The validity of this procedure can be questioned. However, we find that the two extracted potentials $\psi_i^{-1}(E-M_i-K_i)\psi_i$ are very nearly equal to *their* average mass potentials, so that the procedure seems entirely self-consistent. We would conjecture that the use of the average mass leads to additional SU(3)-breaking effects of order $(m'-m/m'+m)^2 \sim 0.05$.

It has been previously noted[1,9,13] that the main source of these quark-exchange-generated potentials is the color hyperfine interaction. We have confirmed this by studying the extracted potentials as a function of the hyperfine strength. The conclusion that color electric effects are small can also be reached by a calculation of the intermeson adiabatic potential due to H_{SI} of Eq. (2) using methods which generalize those reported in Appendix D of Ref. 1. Our conclusions regarding these potentials are thus not very sensitive to our use of the questionable $\mathbf{F}_i \cdot \mathbf{F}_j$ confinement potentials.[11]

Before actually using these potentials in the coupled-channel equations, we expand their ranges to make them more realistic. We argue that this *ad hoc* treatment is justified by the inability of the nonrelativistic quark model to predict the correct charge radii of the ground-state mesons and baryons. Since the intermeson potentials are generated by quark exchanges, their ranges are determined by overlaps of $q\bar{q}$ wave functions and hence by the $q\bar{q}$ radii. Thus, although we consider the *relative* strengths and ranges of the potentials of Fig. 3 to be useful predictions, we will expand their absolute ranges by the ratio of the observed to predicted meson charge radii $(\langle r_K^2 \rangle_{\text{expt}}^{1/2} / \langle r_K^2 \rangle_{\text{th}}^{1/2} \simeq 2)$ while decreasing their strengths by a universal factor η. This prescription can certainly be questioned (we consider it to be the weakest element of our analysis), so we would like to add one more observation in its support. It has been argued that the $q\bar{q}$ wave function of the quark model correctly represents the "hadronic core" of the mesons, with the deficit in the observed charge radius being supplied by vector-meson dominance. While this may be, we note that purely hadronic scattering is known empirically to be controlled by essentially the same radius as observed electromagnetically. For example, the momentum transfer dependence of high-energy pp and πp scattering can be well described by the convolution of the *electromagnetic* form factors of the scattering particles.[21] Our method thus leads to results consistent with the requirement that hadronic scattering processes, such as those being considered here, be controlled by the electromagnetic radii.

Since we do not know what to expect for the factor η, we have determined it from a fit to the low-energy $I=2$ $\pi\pi$ phase shifts (see Sec. IV), finding $\eta \simeq 0.5$ (with an error of ± 0.1). With the six adjusted potentials

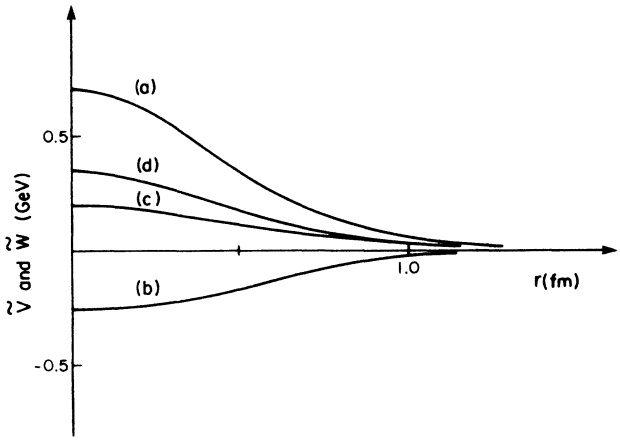

FIG. 4. Some physical potentials, including (a) $\tilde{V}$ for $(\pi\pi)^{I=2}$, (b) $\tilde{V}$ for $(\pi\pi)^{I=0}$, (c) $\tilde{W}$ for $(K\bar{K})^{I=0} \leftrightarrow (\eta\eta)^{I=0}$ and $(K\bar{K})^{I=1} \leftrightarrow (\pi\eta)^{I=1}$, (d) $\tilde{V}$ for $(\pi\eta)^{I=1}$. Note that $\tilde{V}$ for $(K\bar{K})^{I=0}$ and $(K\bar{K})^{I=1}$ are equal and very small.

$\tilde{V}_m(r) = \eta V_m(r/2)$ and $\tilde{W}_m(r) = \eta W_m(r/2)$ we can then predict using Eqs. (32)–(34) the physical pseudoscalar-pseudoscalar potentials we require. Figure 4 shows a selection of such potentials. For computational simplicity, in Sec. IV we will replace these potentials by a set of approximately equivalent square-well potentials.

To complete our coupled-channel approximation to $qq\bar{q}\,\bar{q}$ dynamics, we finally add in the effect of the annihilation potentials Ω_{ij} which couple the meson-meson channels to the (closed) $q\bar{q}$ $^3P_0$ channels as shown in Fig. 1(a). These potentials are described in Appendix B.

C. Solution of the coupled-channel equations

The coupled-channel equations (20), with annihilation channels added on, are sufficiently simple that we have chosen to solve them by direct numerical integration of the radial Schrödinger equation. In the N-channel problem, if there is one open channel, then, for an arbitrary initial slope of the open-channel wave function, the problem is solved once a set of initial slopes of the N-1 closed channels is found which leads to their having damped wave functions at large r: the asymptotic wave function allows one to read off the phase shift of the open channel. If there are two (n) open channels, then such solutions must be found for two (n) linearly independent initial slopes for each of the open channels. Linear combinations of these solutions can then be constructed corresponding to various initial conditions (e.g., an incoming plane wave only in the first open channel). In this way one can extract the complete S matrix.

IV. COMPARISON TO EXPERIMENT

A. General comments

One of the most striking successes of the $K\bar{K}$ molecule picture will be that it makes it obvious why the S^* and δ both lie just below $K\bar{K}$ threshold, bearing somewhat the same relation to it that the deuteron does to the pn

threshold. At the same time one can easily understand why every threshold does not harbor a bound state: in closely related channels such as $\pi\pi$ and πK the delicate binding is overwhelmed by the kinetic energy of the light meson, while in others it can be upset by a change in dynamics that provides an insufficiently attractive potential. That binding might occur in the channel with $J^{PC_n}=0^{++}$ also seems natural, at least in retrospect, simply because these are the quantum numbers of the $qq\bar{q}\,\bar{q}$ ground states in the absence of meson-meson interactions: namely, two pseudoscalar mesons in a relative S wave. (Dynamical calculations are of course required to show that the potential between these two pseudoscalar mesons is sufficiently attractive to bind them, and that this sufficient attraction occurs in the cryptoexotic but not the exotic channel.)

Another qualitative feature of these states which will be automatically explained by the $K\bar{K}$ picture is their small widths. (They are small relative to the norm, but they are *very* small relative to the expectation for a $q\bar{q}$ $^3P_0$ state; see the Introduction.) That $K\bar{K}$ molecules might naturally have narrow widths is mostly easily seen by imagining the limit in which their (already small) binding energy E_B approaches zero. The tail of such a $K\bar{K}$ wave function behaves as $\psi_{K\bar{K}}(r_{K\bar{K}})\sim r_{K\bar{K}}^{-1}\exp(-\sqrt{m_K E_B}\,r_{K\bar{K}})$ so that in this limit the K and $\bar{K}$ spend almost none of their time in the neighborhood of $\mathbf{r}_{K\bar{K}}=0$. As a result they can neither exchange quarks ($K\bar{K}\to\pi\eta$) nor annihilate them ($K\bar{K}\to\pi\pi$) so that the bound state would become increasingly stable against decay as it becomes more weakly bound. (A quantitative discussion of these effects appears below.)

The last easily understood qualitative feature of these states which will emerge from our analysis is their special relationship to the $K\bar{K}$ channel, and more generally to $s\bar{s}$ quarks. At the crudest level such a special relationship would be expected simply from the dominantly $K\bar{K}$ composition of the states, in stark contrast to the expectation for an (ω,ρ)-like doublet with no valence $s\bar{s}$ pairs. Somewhat more specifically, the $K\bar{K}$ molecule picture will naturally explain the dual effects ascribed to these states: their appearance as narrow resonances below $K\bar{K}$ threshold and their association with the large $I=0$ and 1 S-wave $K\bar{K}$ threshold enhancements. From our point of view we can see that these two effects are closely related, but not to be identified. Consider, for example, the $I=0$ channel and imagine that $\Gamma(S^*\to\pi\pi)\ll 2M_K-M_{S^*}$. Then the S^* would appear as a very narrow Breit-Wigner resonance entirely below $K\bar{K}$ threshold. However, the $K\bar{K}$ S wave would still show essentially the same threshold enhancement, which is an effect of the distortion of the free $K\bar{K}$ plane wave by the $K\bar{K}$ effective potential $V_{K\bar{K}}$ and not a *resonance* effect. [Of course, it is caused by the same potential which creates the S^* bound state, and so is *related* to the S^*. The physical origin of such an enhancement is, however, that the potential pulls in the wave function of the $K\bar{K}$ spherical waves of energy $E>0$, thereby increasing the $K\bar{K}$ wave function at the origin, $\psi^E_{K\bar{K}}(0)$. The matrix element for any local $K\bar{K}$ production process will be roughly proportional to $\psi^E_{K\bar{K}}(0)$ and so be enhanced for kinetic energies less than (or of the order of) the depth of $V_{K\bar{K}}$. This effect is well known in the analogous deuteron system where, for example, $pp\to np\pi^+$ shows a huge threshold enhancement.] Other examples of the special relationship of these states to $s\bar{s}$ are the recent observations[7,8] on the decays $\psi\to\omega X$, ρX, and ϕX. These "flavor-tagging" experiments show the expected strong signals in ωf_2, ρa_2, and $\phi f_2'$, but show little if any signal in ωS^* or $\rho\delta$, and a large ϕS^* signal. These results blatantly violate the expectations of the $q\bar{q}$ picture, but are, as we will see, very natural for $K\bar{K}$ molecules.

In many ways we believe that these qualitative successes of the $K\bar{K}$ molecule picture are its best empirical support. In the next few subsections we will not only establish these features, but also find further strong evidence in support of the picture when we analyze it more quantitatively. This analysis will be based on approximate solutions of the coupled-channel equations of Sec. III obtained by replacing the physical potentials $\tilde{V}$ and $\tilde{W}$ (such as those of Fig. 4) by square-well potentials which are approximately phase-shift equivalent at low energy. There is, of course, some ambiguity in defining such an equivalence. One could, for example, either demand equal scattering lengths or a good "global" fit to the low-energy phase shifts. In view of the semiquantitative nature of our model at present, this extra imprecision is of little real consequence. We have in fact used the freedom it allows in choosing a set of "canonical" square-well potentials with universal range $a=0.8$ fm and strengths $V_u^e=+0.57$ GeV, $V_k^e=+0.29$ GeV, $V_s^e=+0.18$ GeV, $V_u^c=-0.43$ GeV, $V_k^c=-0.25$ GeV, and $V_s^c=-0.15$ GeV. Notice that the signs and approximate *relative* strengths of these canonical potentials could just be read off Fig. 3; their absolute strength is controlled by the factor η introduced in Sec. III by fitting to the low-energy $I=2$ $\pi\pi$ phase shift. The annihilation potentials Ω_{ij} we use are also taken to be square wells of this radius with strengths adjusted to give the computed[3,4] $q\bar{q}$ scalar-meson widths, while the $q\bar{q}$ channel was taken to be confined by an infinite square well of range $2a$ (see Appendix B) with a depth, which determines the $^3P_0$ "bare" masses, taken to be a free parameter. (We attempted a fit to the data using the masses predicted by the model of Ref. 3, but they appear to be about 200 MeV too low. This indicates that spin-orbit forces in the P-wave mesons are even smaller than those found in Ref. 3, a situation reminiscent of the P-wave baryons.) The use of these square-well potentials greatly facilitates the numerical solution of the coupled-channel equations while retaining their main features; at present, a more exact treatment is difficult to justify. We will give examples of the sensitivity of our conclusions to these square-well potentials in the following discussions.

B. Evidence from $\pi\pi$ scattering

Studies of S-wave $\pi\pi$, πK, $K\bar{K}$, and KK scattering have a long history, but it is only recently that the very difficult experiments required to study these processes have begun to draw firm conclusions on many of the issues relevant to us.[22,23]

The oldest and simplest such process is $\pi\pi$ scattering, which is essentially elastic up to, but very inelastic above, $K\bar{K}$ threshold. Some measured amplitudes for this system are shown in Figs. 5–7 along with the results of our coupled-channel analysis defined in Sec. III. Figure 5 shows the simplest case of all: the purely exotic $I=2$ $\pi\pi\to\pi\pi$ phase shift.[24] Since, as described in Sec. III B, we used this process to "tune" our model, the quality of the fit cannot be claimed as a success of the calculation. However, we emphasize that the repulsive character of this amplitude, its qualitative shape, and its general magnitude are unambiguous predictions of the model. This one-channel process also allows us to illustrate the effect of one of the simplest sorts of relativistic corrections on our results: Figure 5 shows the predicted $I=2$ phase shift when the wave number k is given not by $m_{\pi\pi}=2(m_\pi+k^2/2m_\pi)$ but rather by $m_{\pi\pi}=2(m_\pi^2+k^2)^{1/2}$, as would happen if we replaced the Schrödinger equation with the Klein-Gordon equation. It seems clear that most of the difference could be absorbed into a small change in the parameter η of Sec. III B.

We now turn from the simplest system to the most complicated: $I=0$ S-wave scattering. This process in principle involves at least seven channels: $\pi\pi$, $K\bar{K}$, $\eta\eta$, $\eta\eta'$, $\eta'\eta'$, $\sqrt{1/2}(u\bar{u}+d\bar{d})\,{}^3P_0$, and $s\bar{s}\,{}^3P_0$. Such a seven-channel approximation to $\pi\pi$ scattering should be useful in the region below about 1.5 GeV where our immediate interest lies. (Above this mass one must also consider the S-wave spin zero vector-vector channels such as $\rho\rho$ and $\omega\omega$ which we have hitherto ignored, the $\pi\pi'$ channel, and possible couplings to scalar glueballs and hybrid states. A comprehensive study of this 00^{++} sector will thus present formidable challenges, making us less than sanguine about the possibility of uncovering a scalar glueball in this mass region.) Figure 6 shows the comparison of this model of elastic $\pi\pi$ scattering with data, demonstrating that the $K\bar{K}$ molecule picture explains the main features of this channel. The broad rise from threshold is due mainly to the combined effects of the attractive $\pi\pi$ potential and a broad[3,4] $I=0$ ${}^3P_0 q\bar{q}$ state with bare mass $\sim$1300 MeV. The sharp resonance below $K\bar{K}$ threshold is the $K\bar{K}$ molecule. This strongly suggests that the observed $f_0(1300)$ resonance[25] is the ${}^3P_0$ $q\bar{q}$ state. Our model is not reliable at 1500 MeV, since by such a mass new channels such as $\rho\rho$ might be very important; we therefore do not show this region. However, our solution does exhibit a small loop at about 1500 MeV associated with the f_0', showing that the dynamics has produced a *new* scalar meson. We emphasize that the couplings of the ${}^3P_0$ $q\bar{q}$ states were completely predicted by earlier analyses.[3,4] It should also be noted that, as promised in the Introduction, the $K\bar{K}$ molecule picture not only explains the existence of the S^* just below $K\bar{K}$ threshold, but also its width, giving $\Gamma(S^*\to\pi\pi)\approx 38$ MeV, near to the tabulated value[25] of 34 ± 6 MeV.

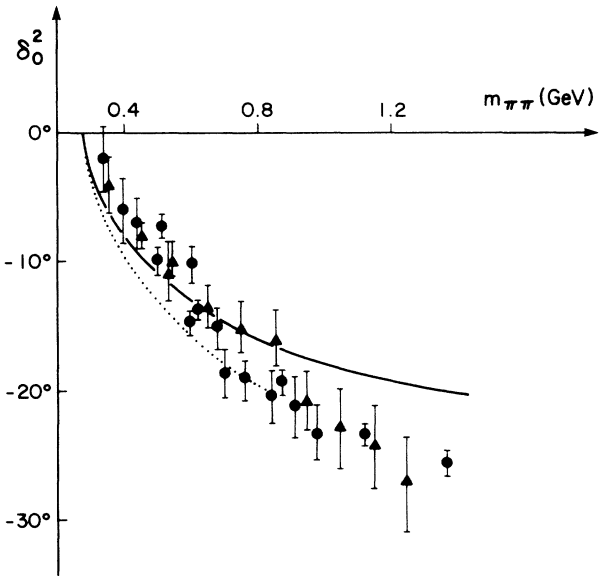

FIG. 5. The experimental (Ref. 24) $I=2$ $\pi\pi$ elastic phase shift compared to theory; the dotted curve corresponds to using a relativistic dispersion relation.

Of particular interest is the $K\bar{K}$ elastic phase shift. Since the two-channel S matrix must have the form

$$S=\begin{pmatrix} \eta e^{2i\delta_1} & i(1-\eta^2)^{1/2}e^{i(\delta_1+\delta_2)} \\ i(1-\eta^2)^{1/2}e^{i(\delta_1+\delta_2)} & \eta e^{2i\delta_2} \end{pmatrix} \tag{38}$$

the elastic $K\bar{K}$ phase shift $\delta_{K\bar{K}}$ can be obtained by subtracting the $\pi\pi\to\pi\pi$ phase shift $\delta_{\pi\pi}$ from the $\pi\pi\to K\bar{K}$ phase $\delta_{\pi\pi}+\delta_{K\bar{K}}$. The $K\bar{K}$ molecule picture shows the characteristic drop from 180° expected for a bound state (Fig. 7); experiment[26–28] is ambivalent because it is very difficult to find a phase with which to interfere $\pi\pi\to K\bar{K}$ near threshold, but the experiment[26,27] which claims the greatest sensitivity in this region sees a drop. Indeed, on this basis it was suggested in Ref. 27 that the most likely interpretation of the S^* was as a $K\bar{K}$ bound state. Figure 7(c) shows the $K\bar{K}$ elastic Argand diagram. Several additional comments on Figs. 5–7 are in order.

(1) It will have been clear to the reader from Sec. III B that there are substantial uncertainties in deducing the coupled-channel equations for our $qq\bar{q}\,\bar{q}$ calculations. Figures 8, when compared with Fig. 6(b'), show how the $I=0$ $\pi\pi$ scattering Argand diagrams vary with changes in our coupled-channel parameters. Figure 8(a) shows that the exotic potentials have little influence: even reducing their strengths by a factor of 2 only makes the phase shifts rotate slightly counterclockwise below 1 GeV. Figure 8(b) shows more sensitivity to the cryptoexotic potentials, as expected. On comparing Figs. 6(b') and 8(b), it is clear that a small adjustment of V^c would produce an Argand diagram with a phase at $K\bar{K}$ threshold identical to that shown in Fig. 6(b). This is an illustration of the fact that this feature of the Argand diagram is very difficult to determine (both experimentally and theoretically) since it occurs during the rapid phase motion associated with the S^*. Figure 8(c) shows that our results are not very sensitive to assuming an SU(3)-breaking $s\bar{s}$ pair creation factor λ (see Appendix B): changing from the SU(3) limit value of unity to $\frac{3}{4}$ produces only modest changes in Fig. 6(b'). Finally, Fig. 8(d) shows that our results are quite sensitive to the annihilation amplitude Ω. We will discuss this point further in

Sec. IV E below.

(2) Despite its name and location, the "$K\bar{K}$ molecule" is not a simple $K\bar{K}$ bound state. Its stability is dependent on its couplings to the other $I=0$ channels and at $E=M_{S^*}$ the coupled-channel wave function has substantial components of the other states.

(3) The addition of the $q\bar{q}$ $^3P_0$ states as closed channels provides not only much of the $S^* \to \pi\pi$ decay amplitude (some also comes from second-order processes such as $K\bar{K} \to \eta\eta \to \pi\pi$ via the large Okubo-Zweig-Iizuka- (OZI-) rule violation in the η wave function [see Fig. 1(c)]), but also a significant source of stabilization to the $K\bar{K}$ bound state.[29]

(4) Unlike a $q\bar{q}$ resonance interpretation, in the $K\bar{K}$ molecule picture the "$\pi\pi$ resonance" below $K\bar{K}$ threshold and the dramatic threshold enhancement in $K\bar{K}$ production are intimately related but not inseparable: even if the effective $K\bar{K}$ potential were reduced to the point that the bound state disappears, the large threshold enhancements seen in $K\bar{K}$ production (see below) would remain. (They would then be associated with a $K\bar{K}$ phase that rose rapidly from 0 to just under 90° and then returned to zero instead of one that dropped from 180° through 90° to zero.) Moreover, for fixed M_{S^*}, even if the $S^* \to \pi\pi$ coupling were tuned to zero there would still be essentially the same $K\bar{K}$ threshold effect. This corresponds to our earlier remark that the S^* (and δ) are associated with, but not to be identified with, the $K\bar{K}$ threshold enhancements.

C. Evidence from production experiments

At this time it has been possible to extrapolate to on-shell π exchange but not to on-shell K or η exchange to

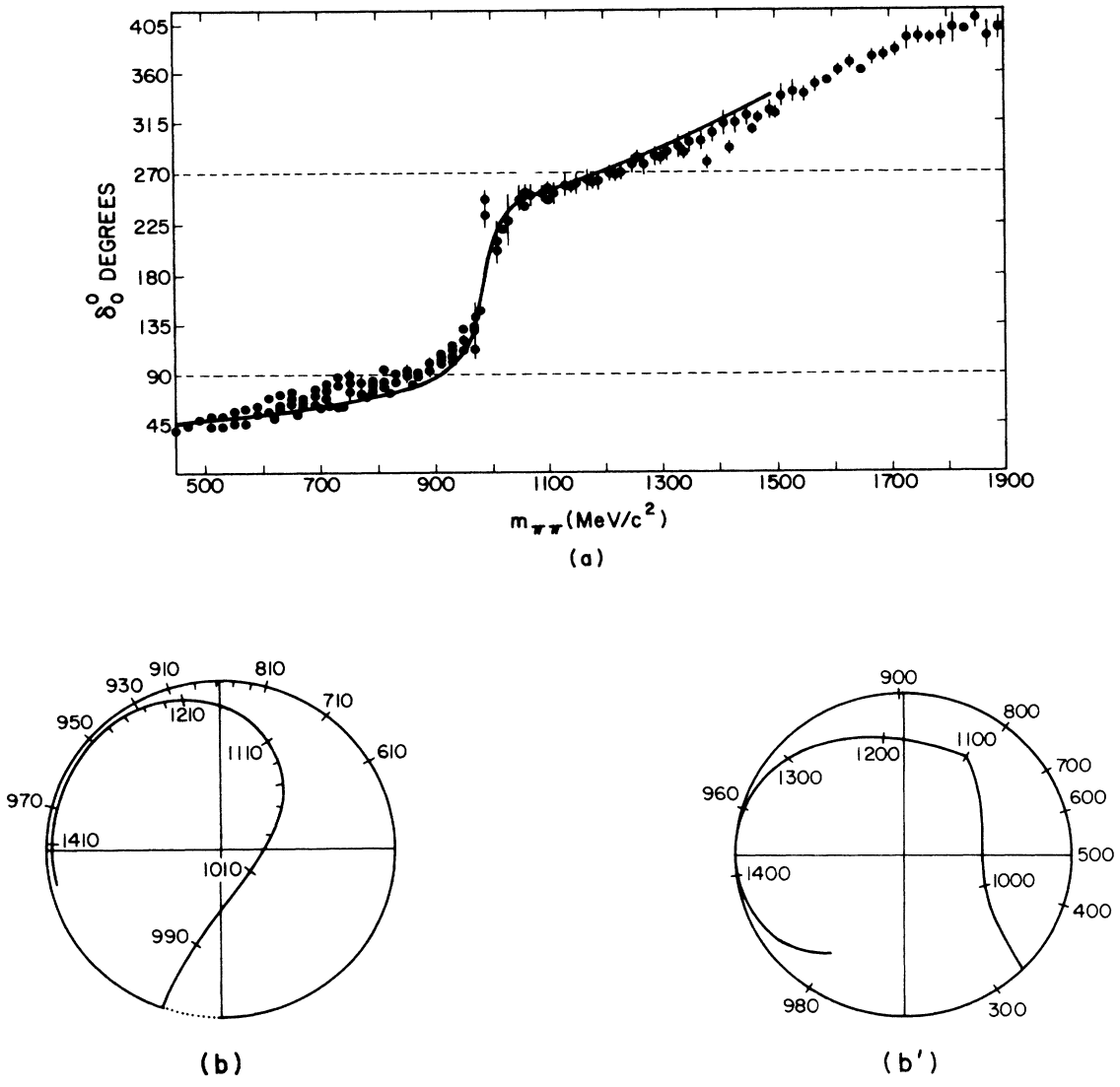

FIG. 6. (a) The $I=0$ $\pi\pi$ phase shift compared to the $K\bar{K}$ molecule picture; the data correspond to various analyses of the first of Refs. 23. (b) The measured $I=0$ $\pi\pi \to \pi\pi$ Argand diagram (from the same experiment). (b') The predicted $I=0$ $\pi\pi \to \pi\pi$ Argand diagram.

study directly coupled-channel meson-meson scattering. Our predicted amplitudes for the $I=1$ coupled-channel ($\pi\eta, K\bar{K}, \pi\eta', I=1\ q\bar{q}\ ^3P_0$) system shown in Fig. 9 cannot therefore be directly compared to data. However, these results are very useful for demonstrating the physics in operation in this channel. In particular, we see that our model predicts a δ just below $K\bar{K}$ threshold to be the partner of the S^*, as well as a mainly $q\bar{q}$ state $a_0(1300)$ to join the scalar-meson nonet. The δ is predicted to be about 60 MeV wide at threshold, in reasonable agreement with the experimental value of 57 ± 11 MeV. (Note, however, that our predicted resonance is far from having a Breit-Wigner line shape, so this comparison must be treated with caution.) We see that, in contrast with the $f_0(1300)$, the $a_0(1300)$ creates a quite small disturbance in the Argand diagram; this has consequences to which we turn below. Figure 10 shows the sensitivity of our results to the same variations that were considered in Fig. 8.

For further comparison of the $K\bar{K}$ molecule picture to experiment, we must turn our attention to various production processes in which S^* and δ effects can be seen. We have begun a quantitative study[30] of multichannel production along the lines suggested in Appendix E, and intend to report on our detailed analysis of the phenomenology of S-wave pseudoscalar-pseudoscalar production

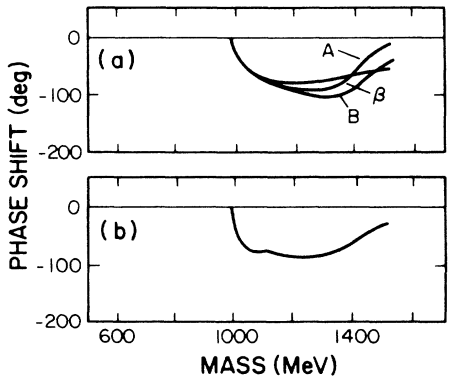

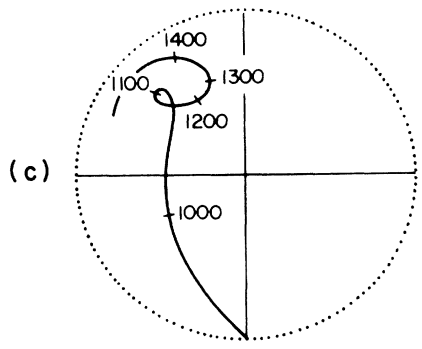

FIG. 7. (a) The " measured" (Ref. 26) $I=0$ $K\bar{K}\to K\bar{K}$ phase shift obtained from $\pi\pi\to K\bar{K}$ and $\pi\pi\to\pi\pi$; A, B, and β correspond to various $\pi\pi\to\pi\pi$ phase-shift solutions. (b) The prediction of the text for (a). (c) The $I=0$ $K\bar{K}$ elastic scattering Argand diagram.

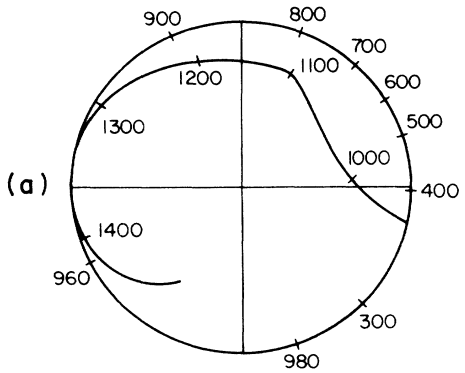

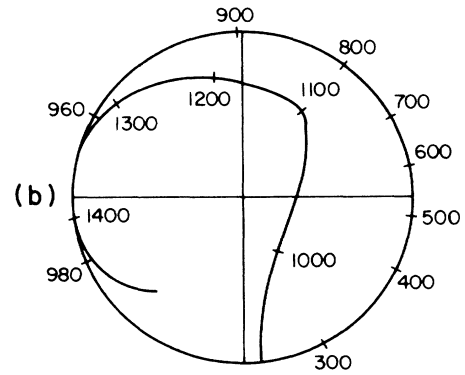

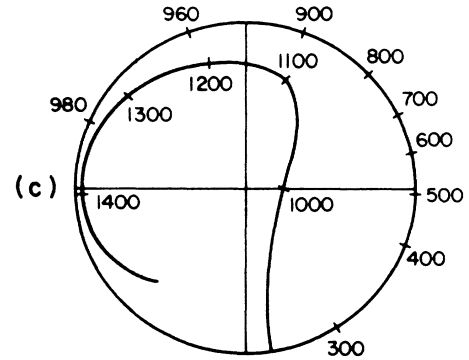

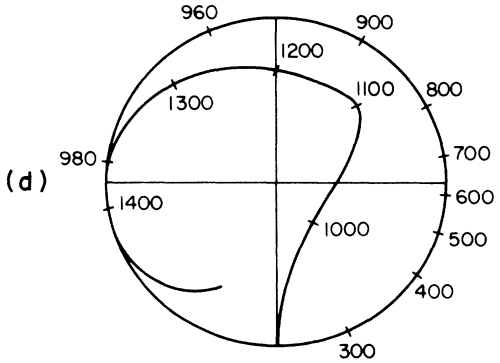

FIG. 8. Variation of the $I=0$ $\pi\pi$ Argand diagram (compare with Fig. 6) with changes in the coupled-channel potentials: (a) $V^e\to0.5$ of its canonical value, (b) $V^c\to0.8$ of its canonical value, (c) $\lambda\to\frac{3}{4}$, (d) Ω decreases from 0.11 GeV to 0.10 GeV.

forthwith. We would nevertheless like to discuss qualitatively some particularly interesting processes here. For orientation, let us consider a single-channel $K\bar{K}$ problem with a $K\bar{K}$ bound state. The simplest S^* and δ effects occur in the decay of a 0^{++} resonance into the $K\bar{K}$ channel. As shown in Appendix B, the rate for such a process will be enhanced by the "wave function at the origin effect" mentioned in Sec. IV A above:

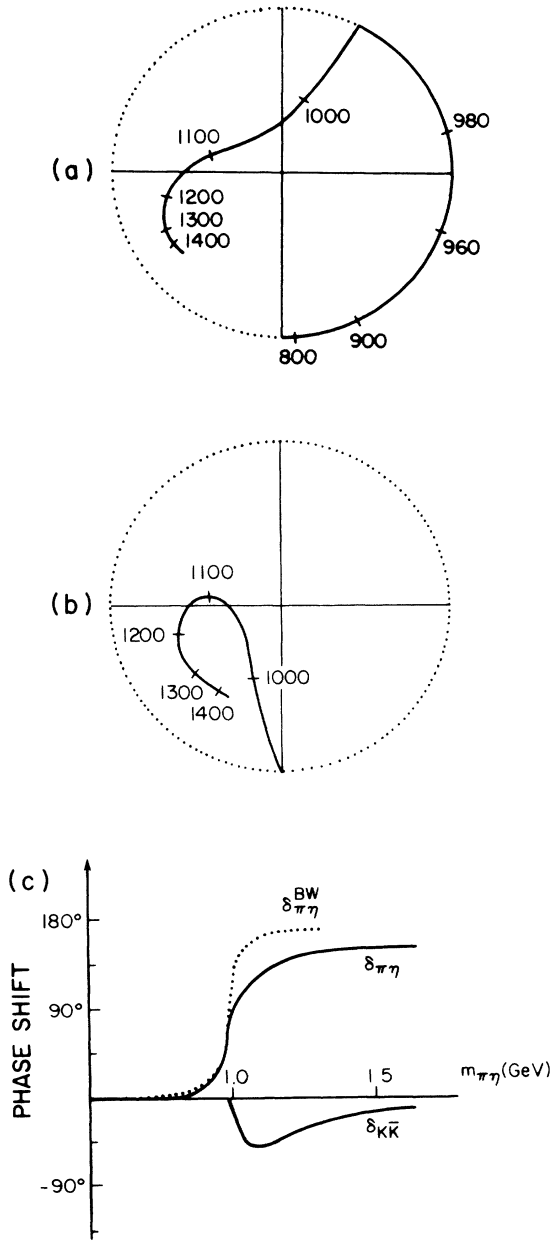

FIG. 9. (a) The predicted coupled-channel Argand diagram for $\pi\eta$ elastic scattering. (b) The predicted Argand diagram for $K\bar{K}$ elastic scattering with $I=1$. The dotted line shows the unitarity circle. (c) The $\pi\eta$ and $K\bar{K}$ elastic phase shifts; shown to aid comparison is a simple Breit-Wigner shape with energy-independent mass and width set to the Particle Data Group values (Ref. 25) for the δ.

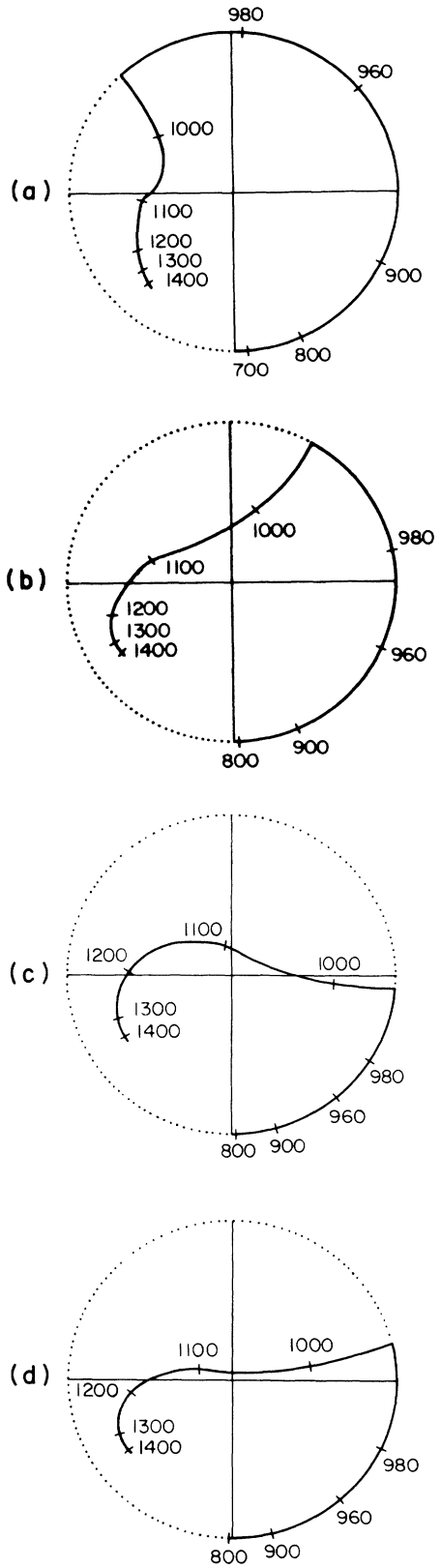

FIG. 10. Variation of the coupled-channel Argand diagram for elastic $\pi\eta$ scattering with changes in the potentials (compare with Fig. 9): (a) $V^e \to 0.5$ of its canonical value, (b) $V^c \to 0.8$ of its canonical value, (c) $\lambda \to \frac{3}{4}$, (d) Ω decreases from 0.11 GeV to 0.10 GeV.

$$\Gamma(S\to K\bar{K})=\Gamma(S\to K\bar{K})^{\text{free}}\left|\frac{\psi_p(0)}{\psi_p^{\text{free}}(0)}\right|^2$$
$$\equiv\Gamma(S\to K\bar{K})^{\text{free}}d(m_{K\bar{K}})\ , \tag{39}$$

where $p=(\frac{1}{4}m_{K\bar{K}}^2-m_K^2)^{1/2}$ is the center-of-mass momentum of the kaon pair, ψ_p is the S-wave wave function with asymptotic momentum p, and the superscript "free" denotes a quantity with $V_{K\bar{K}}=0$. For a square well of depth V_0 and range a,

$$d(m_{K\bar{K}})=\frac{p_0^2}{p_0^2\cos^2(p_0a)+p^2\sin^2(p_0a)}\ , \tag{40}$$

where $p_0=\sqrt{p^2+m_KV_0}$; if the square well has a single bound state with binding energy E_B then this can be rewritten as

$$d(m_{K\bar{K}})=\frac{m_{K\bar{K}}-2m_K+V_0}{m_{K\bar{K}}-2m_K+E_Bf(m_{K\bar{K}})}\ , \tag{41}$$

where

$$f(m_{K\bar{K}})=\frac{V_0}{E_B}\cos^2\left\{\left[\frac{m_{K\bar{K}}-2m_K}{V_0}+1\right]^{1/2}\times\left[\frac{\pi}{2}+\left[\frac{E_B}{V_0}\right]^{1/2}\right]\right\}. \tag{42}$$

Figure 11 shows how the width of a particle with fixed intrinsic coupling constant varies with its mass. The effect is a prototypical $K\bar{K}$ threshold enhancement.

These effects will also be present in multibody decays $X\to YK\bar{K}$ where X is any decaying state and Y may represent a collection of final-state particles. In general, of course, there will be final-state interactions between the K and $\bar{K}$ and Y, but in the simplest case where they can be ignored the final-state relative coordinate wave function will be of the form

$$\psi_Y(y)\psi_{K\bar{K}}(r)e^{+i\mathbf{P}\cdot\mathbf{R}}\ ,$$

where the coordinates y are internal to Y, r is the $K\bar{K}$ relative coordinate, and $\mathbf{R}$ is the relative coordinate between the $K\bar{K}$ center of mass and that of Y. In this case, in the same approximation as above, the enhancement factor $d(m_{K\bar{K}})$ of Eq. (40) applies to the $K\bar{K}$ subspectrum of the more complex decay.

Simple one-channel models of these types have been used to discuss several peculiar features of hadronic decays near thresholds.[31,32] The basic idea is an old one which dates back to Fermi.[31] The multichannel formalism we have developed here can be applied to such decays to make their treatment more realistic. In the simplest case the decay might "feed" a single channel which would then scatter into other channels on its way out of the interaction region. In general the decay can feed many channels so that very complex behavior can result. See, for example, the behavior of the $f_0(1300)$ and $a_0(1300)$ resonances in Figs. 6, 7, and 9.

A more typical production process is shown in Fig. 12 in which the $I=1$ δ channel is studied[33] via $K^-p\to\pi^-\eta\Sigma^{*+}(1385)$ and $K^-p\to K^-K^0\Sigma^{*+}(1385)$. To the extent that they are dominated by K^0 exchange they

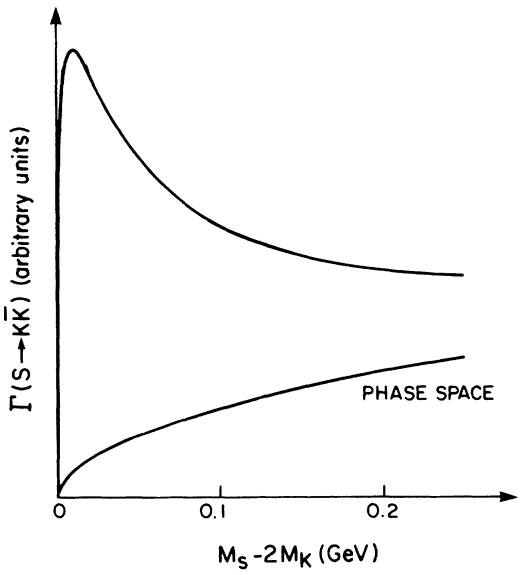

FIG. 11. $\Gamma(S\to K\bar{K})$ according to Eq. (39) for fixed intrinsic $S\to K\bar{K}$ coupling showing the effect of the enhancement factor (40); the curve corresponds to a potential of range 0.8 fm which has a 20-MeV deep bound state of $K\bar{K}$.

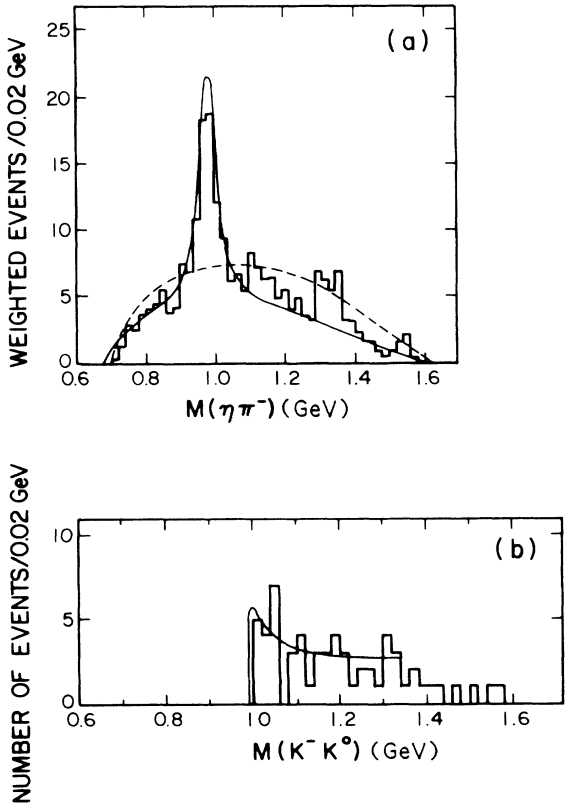

FIG. 12. $\pi\eta$ and $K\bar{K}$ production in (a) $K^-p\to\pi^-\eta\Sigma^{*+}$ and (b) $K^-p\to K^-K^0\Sigma^{*+}$ from Ref. 33. The curve in (b) is from Eq. (43).

are analogous to the π-exchange-dominated $\pi N \to \pi\pi N$ and $K\bar{K}N$ reactions, and lead to information on $K^- K^0 \to K^- K^0$ and $\pi^- \eta$. The $I=1$ coupled-channel results of Fig. 9 cannot, of course, be applied directly to this unextrapolated data which, even assuming K^0 exchange, depends on the baryon vertex and on the amplitude for off-shell $K^- K^0_{\text{virtual}}$ scattering. However, the $K\bar{K}$ molecule picture can still say a great deal about such data.

To discuss such production experiments we need to extend our coupled-channel equations to include source (i.e., driving) terms. By this device an outgoing $I=1$ coupled-channel system (for example) can be produced as a part of some more complex dynamical process. For orientation, let us once again begin with a single-channel approximation. As shown in Appendix E, the driven single-channel problem produces an outgoing wave with an intensity enhanced by the same "wave function at the origin" factor (40) as is present in single-channel decays. This threshold enhancement effect in the one-channel approximation

$$\frac{d\sigma}{dm_{K\bar{K}}} = d(m_{KK}) \frac{d\sigma^{\text{free}}}{dm_{K\bar{K}}} \tag{43}$$

is compared to the data in Fig. 12 (by assuming $d\sigma^{\text{free}}/dm_{K\bar{K}}$ is proportional to $K\bar{K}$ phase space).

Before closing this qualitative discussion of S-wave pseudoscalar-pseudoscalar production, we want to quickly touch on two other related processes and their interpretation.

(1) We have mentioned that $\psi \to \phi S^* \to \phi\pi\pi$ is seen.[7,8] We expect that this process can be modeled by our coupled-channel equations with a driven term in the OZI-rule-allowed $K\bar{K}$ channel, or, perhaps, by one in the OZI-rule-allowed $^3P_0$ $s\bar{s}$ channel. That $S^* \to \pi\pi$ is seen in this way is probably due to the very large inelasticity of the low-energy coupled $I=0$ $\pi\pi - K\bar{K}$ system (see Figs. 6 and 7). Figure 13 shows a preliminary result from Ref. 30 based on driving the $I=0$ sector with a source in the $K\bar{K}$ channel.

(2) The process $\eta(1440) \to K\bar{K}\pi$ has already been discussed in the one-channel approximation in the $K\bar{K}$ molecule picture.[32] It was argued that the very strong $\delta\pi$ signal seen experimentally[7,8] is not inconsistent with the absence of an $\eta\pi\pi$ signal since the δ signal would arise from a $K\bar{K}$ "wave function at the origin" effect.

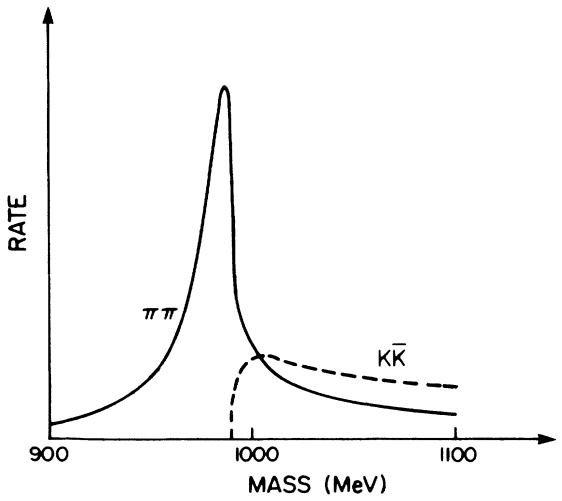

FIG. 13. A preliminary result from Ref. 30 showing the rate of production of $\pi\pi$ and $K\bar{K}$ when the coupled-channel equations of Sec. IV B are driven by a source in the $K\bar{K}$ channel as discussed in Appendix E; data (Refs. 7 and 8) on $\psi \to \phi\pi\pi$ and $\phi K\bar{K}$ are in qualitative agreement with these curves, which display an apparently very large violation of the OZI rule.

D. Where are the $q\bar{q}$ scalar mesons and the scalar glueballs?

It seems fair to claim (see Figs. 6 and 7) that our model has produced a reasonable qualitative understanding of the $I=0$ channel, including the observed $f_0(1300)$ meson. There are also reasons to believe that the elusiveness of its $I=1$ partner $a_0(1300)$ may be associated with the very small off-center loop the a_0 produces in the Argand diagram of Fig. 9; we hope to make more detailed comments on this issue later.[30] The effects on $\pi\pi$ scattering of the $s\bar{s}$ state with mass around 1500 MeV cannot, as mentioned earlier, be predicted reliably since at this high mass channels such as $\rho\rho$ may be important. However, the model does predict reliably that this state should appear in $K\bar{K}$ production experiments.[30] It remains to study πK scattering to demonstrate that our picture can account for the structures seen in this system. At this point we can only say that SU(3) symmetry would suggest that this comparison will be satisfactory. Thus we do not believe the $K\bar{K}$ molecule interpretation of the S^* and δ creates a problem for the quark model by producing a "hole" in the $L=1$ SU(6) supermultiplet. On the contrary, we believe the calculations presented here indicate a possible resolution of long-standing puzzles associated with the $^3P_0$ nonet.[2,22]

The identification of glueballs in the $I=0$ meson sector above 1 GeV is clearly going to be very complicated. Nevertheless, this analysis allows us[30] to compare expected structures in channels such as $\pi\pi \to \eta\eta$, $\eta\eta'$, and $\eta'\eta'$ with those recently observed.[34]

E. Other interpretations of the data

We have already discussed at considerable length the interpretation of the S^* and δ in the bag model and its relation to the one advocated here. In this section we would like to mention some other alternatives.

The most economical possibility is that the S^* and δ can be associated with the $^3P_0$ $q\bar{q}$ nonet. Tornquist in Ref. 35 attempts to make such an association by invoking unitarity shifting and narrowing mechanisms similar to those of Flatté in Ref. 36. Indeed, in this picture the intrinsic widths of the scalar mesons are all in the 500–1000-MeV range, and narrow structures (recall $\Gamma_{S^*} \simeq 35$ MeV) are produced by the cusplike behavior of amplitudes near thresholds. Figure 14 shows that this possibility is quite realistic. They show the $I=0$ and 1 Argand diagrams with all the quark-exchange potentials

set equal to zero, i.e., with pure $q\bar{q}$ resonance dynamics. The $I=1$ channel in this limit has an a_0 which has been pushed down below $K\bar{K}$ threshold and narrowed by the Flatté-Tornquist mechanism. $I=0$ shows a similar behavior. The resulting amplitudes show many similarities to those of the $K\bar{K}$ molecule interpretation: compare Fig. 15 with Fig. 9(b). There are, however, many ways to discriminate between this picture and the $K\bar{K}$ molecule interpretation. The most fundamental is that we require two additional states: the Flatté-Tornquist mechanism pulls the $^3P_0$ states down to $K\bar{K}$ threshold, but cannot produce an additional state. Thus confirmation of the existence of an $a_0(1300)$ or an $f_0'(1500)$ would strongly support the $K\bar{K}$ molecule picture.

Although strictly speaking it is not an "interpretation," we would also like to mention the recent very extensive study of the coupled-channel $I=0$ system by Au, Morgan, and Pennington.[22] They performed a simultaneous and unitary fit to a very wide body of data based on a minimal set of K-matrix poles. Their conclusion was that the data required not only a broad $f_0(1300)$-type pole, but also a very complex two-pole structure near $K\bar{K}$ threshold. One possibility, which they have emphasized, is that one of these poles is a $K\bar{K}$ bound state and the other is a new, very narrow state (possibly a scalar glueball). It might also be that the complex behavior they see is a manifestation of the dual nature of the "S^* effect": it is a Breit-Wigner-type resonance in $\pi\pi$ *and* a threshold enhancement in $K\bar{K}$. We hope to comment on this interpretation of their result later.[30]

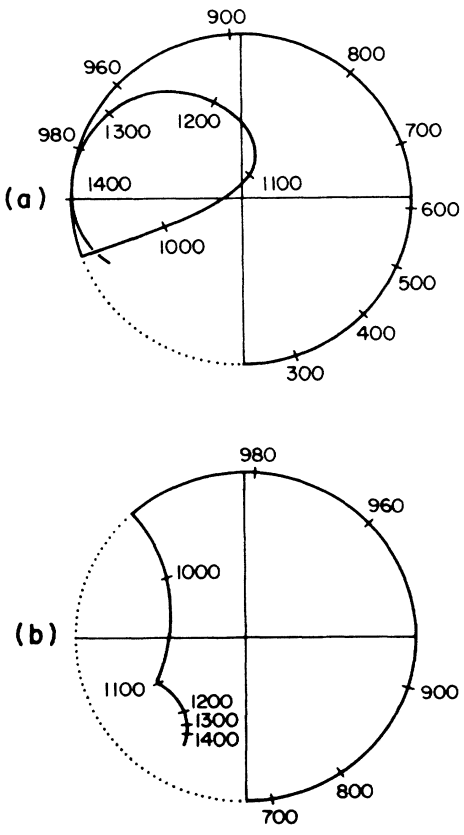

FIG. 14. (a) The $I=0$ $\pi\pi$ elastic Argand diagram with Ω at its canonical value, but with V^c and V^e set to zero. (b) The $\pi\eta$ elastic Argand diagram under the same conditions as in (a).

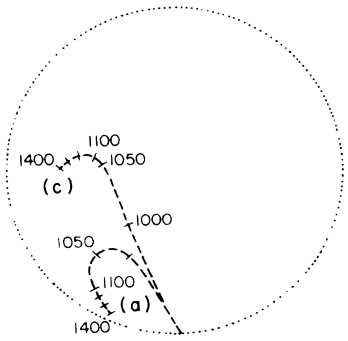

FIG. 15. The elastic $K\bar{K}$ Argand diagrams of the resonance fits (a) and (c) of Flatté in Ref. 36.

V. FUTURE PROSPECTS AND CONCLUSIONS

We believe that the results presented here, along with recent experimental findings we have discussed, make the $K\bar{K}$ molecule interpretation of the S^* and δ more plausible than ever. Nevertheless, further investigations are required before it can be accepted.

On the part of theory, we hope we have made it clear that much remains to be done at the fundamental level of understanding the dynamics of the $qq\bar{q}\,\bar{q}$ system. Given the framework we have adopted, it would be possible to improve substantially upon the accuracy of the solutions we have obtained. However, we have taken the point of view here that this is not warranted in view of the many weaknesses of our model. Rather, it is in seeking remedies for the flaws of the model listed in Sec. II that we feel there is the best chance for improvements. In another vein, assuming the validity of the basic $K\bar{K}$ molecule picture, there is a great deal of room for phenomenological work on the predicted properties of these systems, and in particular on characteristics which can distinguish between the $q\bar{q}$ and $K\bar{K}$ interpretations. We have already mentioned in Sec. I an example[6] of such work on the $\gamma\gamma$ couplings of the S^* and δ which favors the $K\bar{K}$ molecule interpretation. There are also many ramifications of the existence of substantial meson-meson potentials which remain to be worked out. For example, it has recently been suggested[37] that various $I=0$ $\pi\pi$ threshold enhancements have their origin in the attractive $\pi\pi$ potential (see Fig. 4). It may also be that other "bumps" seen near thresholds [e.g., the $I=0$ $J^{PC}=1^{++}$ effect seen in $K^*\bar{K}$, low mass $K\pi$ effects,[38] the series of vector-vector peaks[39] seen in $\gamma\gamma\to V_1V_2$, the $\Lambda(1405)$ baryon, etc.] are produced by residual hadron-hadron potentials.

There is at the same time a very large scope for improvements in our experimental knowledge of such effects. Especially once theory has exposed more clearly the expected behavior of $K\bar{K}$ molecules, the completion of experiments such as the flavor-tagging measurements mentioned above should clarify matters considerably.

There is in addition much room for improvement in standard hadronic production experiments, as well as the possibility of experiments which can directly address novel features of the $K\bar{K}$ molecules picture. For example, it has been suggested[40] that the forward cross section for production of high-energy S^*'s and δ's should, if they are $K\bar{K}$ molecules, have a dramatically distinct dependence on the atomic number of their production target from, e.g., the $q\bar{q}$ tensor mesons.

Given the improvements we can expect in both theory and experiment, one might hope that the nature of the S^* and δ will be established in the relatively near future. If they are indeed $K\bar{K}$ molecules, then one would anticipate that the quark exchange forces which bind them might be important not only in this isolated system, but also in other multiquark systems. The most important such example is undoubtedly the nucleus itself.

ACKNOWLEDGMENTS

This work has benefited from discussions with innumerable people over several years. Ted Barnes has borne the burden of more of these discussions than anyone else, and has made many important suggestions. Kevin Dooley, Greg Grondin, Kim Maltman, and Eric Swanson have played similar roles. We have also been helped enormously by insightful questions posed along the way by Bob Jaffe, Harry Lipkin, and Michael Peskin, as well as by Joe Macek's advice on how to markedly increase the efficiency of our solution of the coupled-channel equations. Finally, we have to admit that this project would probably never have been completed if L. Cameron and K. Bergsagel had not begun to doubt whether completing it was possible.

APPENDIX A: THE OPERATORS $\tilde{r}^{-1}$ AND $\tilde{\delta}^3(\mathbf{r})$

Relativistic corrections (including momentum dependence of the interactions, off-shell effects, and the field-theoretic cutoff intrinsic to the quark model) will smear out all of the operators of the Breit-Fermi limit. Since $\delta^3(\mathbf{r})$ is too singular an operator to be allowed in the Schrödinger equation, it is essential to consider its smearing; for the less singular $1/r$ potential we have simply found it more convenient.

We take for both of these smeared operators Gaussian forms:

$$\tilde{\delta}(\mathbf{r})=\frac{\sigma^3}{\pi^{3/2}}e^{-\sigma^2 r^2} \tag{A1}$$

and

$$\tilde{r}^{-1}=V_G e^{-\kappa^2 r^2} \tag{A2}$$

Although we expect on general grounds that σ will be of the order of the quark mass, its exact value is unknown and so we treat it as a parameter. Our fits to ordinary meson spectroscopy then give $\sigma=0.92$ GeV. [This parameter is mainly determined by the splitting between the $1\,^1P_1$ meson $b_1(1235)$ and the center of gravity of the $1\,^3P_J$ mesons $a_2(1320)$, $a_1(1260)$, and $a_0(\sim 1300)$.] On the other hand, κ is not a parameter: we choose it to be 0.2 GeV to give approximately the same ratios of expectation values as r^{-1} in the $1S$, $1P$, and $1D$ levels of light quarks in the linear potential of Eq. (2). We could also constrain V_G to give the absolute value of the expectation value of $1/r$ (this would require $V_G \simeq 0.5$ GeV), but in accord with the findings of Ref. 3 we allow V_G to be independently fit to meson spectroscopy as a means of allowing the effective α_s in the $1/r$ potential to differ from that in the hyperfine interaction. This gives $V_G=0.375$ GeV.

APPENDIX B: The $qq\bar{q}\,\bar{q}\leftrightarrow q\bar{q}$ POTENTIALS Ω_{ij}

The meson-meson channels of the text are coupled to $^3P_0\,q\bar{q}$ channels via Fig. 1(b). Since in the SU(3) limit the coupling annihilates two mesons with relative coordinate $\mathbf{r}_M-\mathbf{r}_{\bar{M}}\equiv\mathbf{r}_1$ into a $q\bar{q}$ state with $\mathbf{r}_q-\mathbf{r}_{\bar{q}}\equiv\mathbf{r}_2$ at the point $\mathbf{r}_2=2\mathbf{r}_1$, the coupled channel equations are of the form ($1\leftrightarrow M\bar{M}$, $2\leftrightarrow q\bar{q}$)

$$-\frac{1}{2\mu_1}\tilde{u}_1''(r_1)+\tilde{V}_1(r_1)\tilde{u}_1(r_1)+\Omega(r_1)\tilde{u}_2(2r_1)=E\tilde{u}_1(r_1)\ , \tag{B1}$$

$$-\frac{1}{2\mu_2}\tilde{u}_2''(r_2)+\tilde{V}_2(r_2)\tilde{u}_2(r_2)+\Omega\left[\frac{r_2}{2}\right]\tilde{u}_1\left[\frac{r_2}{2}\right]=E\tilde{u}_2(r_2)\ , \tag{B2}$$

where the $\tilde{u}_i(r_i)$ are the radial wave functions of channel i, the potentials $\tilde{V}_i(r_i)$ include appropriate rest mass and centrifugal barrier terms, and where $\Omega(r)$ is the amplitude for interconversion between the meson-meson system with $r_1=r$ and the $q\bar{q}$ system with $r_2=2r$. It is therefore convenient to set $r_1=r$, $r_2=2r$, and to define new functions

$$\begin{aligned} u_1(r)&=\tilde{u}_1(r),\quad V_1(r)=\tilde{V}_1(r)\ ,\\ u_2(r)&=\tilde{u}_2(2r),\quad V_2(r)=\tilde{V}_2(2r)\ , \end{aligned} \tag{B3}$$

so that Eqs. (B1) and (B2) become

$$-\frac{1}{2\mu_1}u_1''(r)+V_1(r)u_1(r)+\Omega(r)u_2(r)=Eu_1(r)\ , \tag{B4}$$

$$-\frac{1}{8\mu_2}u_2''(r)+V_2(r)u_2(r)+\Omega(r)u_1(r)=Eu_2(r)\ . \tag{B5}$$

The decay rate of a $q\bar{q}$ state S with unit normalized uncoupled radial wave function $u_S(r)$ is easily calculated in this framework. Using continuum states with the asymptotic form

$$u_k(r)\xrightarrow[r\to\infty]{}\sqrt{2/R}\,\sin(kr+\delta) \tag{B6}$$

(R is the radius of the normalization "box") this decay rate is

$$\Gamma=\frac{2\mu_1 R}{k}|\langle k|\Omega|S\rangle|^2\ . \tag{B7}$$

In the absence of a potential V_1 in the channel 1,

$$\langle k|\Omega|S\rangle_{\text{free}}=\sqrt{2/R}\int_0^\infty dr\,\sin(kr)\Omega(r)u_S(r) \tag{B8}$$

but more generally

$$\langle k|\Omega|S\rangle=\int_0^\infty dr\,u_k(r)\Omega(r)u_S(r)\ . \tag{B9}$$

As a simple example, consider the case where V_1 is an attractive potential of constant depth $-V_0$ and range a. Then in the inner region

$$u_k(r)=\left[\frac{2}{R}\right]^{1/2}\frac{\sin(ka+\delta)}{\sin(k'a)}\sin(k'r)\ , \tag{B10}$$

where $k'=\sqrt{k^2+2\mu_1 V_0}$ or, i.e., using $\tan(ka+\delta)=(k/k_0)\tan(k_0a)$,

$$u_k(r)=\left[\frac{2}{R}\right]^{1/2}\frac{\sin(k'r)}{\left[k'^2/k^2\cos^2(k'a)+\sin^2(k'a)\right]^{1/2}}\ . \tag{B11}$$

If we now take $\Omega(r)$ to be a very short-range effect, then only $u_k(r)$ near $r=0$ is relevant and

$$\frac{\Gamma}{\Gamma_{\text{free}}}=\frac{k'^2}{k'^2\cos^2(k'a)+k^2\sin^2(k'a)} \tag{B12}$$

$$=\frac{V_0+E}{V_0\cos^2(k'a)+E} \tag{B13}$$

as in Eq. (40). If $V_1=-V_0$ supports a single weakly bound state, this can be cast into the form of Eqs. (41) and (42).

Next consider the generalization of these remarks when there are multiple coupled meson-meson channels. In this case, as described in Sec. III C, there are as many linearly independent solutions of the $\Omega_{ij}=0$ equations as there are open channels. From these solutions, one can form orthonormal solutions. The decay rates to these final states, or to a particular open channel, can then be calculated in exact analogy to the above single-channel rates.

From (B7), (B8), and the decay rates of Refs. 3 and 4, one can easily deduce the values of the Ω_{ij}'s. They are

$$\begin{aligned}
&\Omega(a_0\to\eta\pi)=2\Omega Z_{\eta\pi},\quad \Omega(a_0\to K\bar{K})=-2\Omega\lambda\ ,\\
&\Omega(a_0\to\eta'\pi)=2\Omega Z_{\eta'\pi}\ ,\\
&\Omega(f_0\to\pi\pi)=-\sqrt{12}\,\Omega Z_{\pi\pi}\ ,\\
&\Omega(f_0\to K\bar{K})=-2\Omega\lambda,\quad \Omega(f_0\to\eta\eta)=\Omega Z_{\eta\eta}\ ,\\
&\Omega(f_0\to\eta\eta')=\sqrt{2}\,\Omega Z_{\eta\eta'},\quad \Omega(f_0\to\eta'\eta')=\Omega Z_{\eta'\eta'}\ ,\\
&\Omega(f_0'\to\pi\pi)=0,\quad \Omega(f_0'\to K\bar{K})=-\sqrt{8}\,\Omega\ ,\\
&\Omega(f_0'\to\eta\eta)=\sqrt{2}\,\Omega Z_{\eta\eta}\lambda\ ,\\
&\Omega(f_0'\to\eta\eta')=-2\Omega Z_{\eta\eta'}\lambda\ ,\\
&\Omega(f_0'\to\eta'\eta')=\sqrt{2}\,\Omega Z_{\eta'\eta'}\lambda\ .
\end{aligned} \tag{B14}$$

Here Ω is a reduced coupling of the SU(3) limit, $Z_{ij}=\sqrt{\mu_{K\bar{K}}/\mu_{ij}}$ (in which μ_{ij} is the reduced mass of the ij system) is a kinematic factor arising from the conversion from (B7) and (B8) to the amplitudes of Refs. 3 and 4, and λ is an empirical factor which can take into account the suppression of $s\bar{s}$ pair creation.

The correct value for Ω can be estimated by comparing (B7) with the corresponding widths predicted in Refs. 3 and 4. These latter predictions are based on fits to known related decays, but are, of course, model dependent. From such a comparison we deduce that $\Omega=0.11\pm0.04$ GeV. In the "canonical" model of the text we used $\Omega=0.11$ GeV, consistent with this prediction.

APPENDIX C: COLOR WAVE FUNCTIONS AND MATRIX ELEMENTS

Our calculations use explicit color wave functions and transformations between various color bases. We quote some useful results here for completeness and to simplify comparisons with related calculations.

The $qq\bar{q}\,\bar{q}$ system can be coupled to an overall color-singlet system in several ways. Three possible orthonormal bases are $(|\bar{3}_{12}3_{34}\rangle,|6_{12}\bar{6}_{34}\rangle)$ in the diquark-antidiquark picture and $(|1_{13}1_{24}\rangle,|8_{13}8_{24}\rangle)$ or $(|1_{14}1_{23}\rangle,|8_{14}8_{23}\rangle)$ in the meson-meson pictures. [$|\bar{3}_{12}3_{34}\rangle$ denotes, for example, that the quarks, particles 1 and 2, are in the antisymmetric representation $\bar{3}$ of $\mathrm{SU}(3)_{\text{color}}$ and the antiquarks, particles 3 and 4, are in the antisymmetric representation **3** of $\mathrm{SU}(3)_{\text{color}}$. In all cases the total color is zero.] The $\bar{3}$, 3, 6, and $\bar{6}$ wave functions are

$$|\bar{3}^\alpha_{q_iq_j}\rangle=\sqrt{1/2}\epsilon^{\alpha\beta\gamma}q_i^\beta q_j^\gamma\ , \tag{C1}$$

$$|3^\alpha_{\bar{q}_i\bar{q}_j}\rangle=\sqrt{1/2}\epsilon^{\alpha\beta\gamma}\bar{q}_i^\beta\bar{q}_j^\gamma\ , \tag{C2}$$

$$|6^\alpha_{q_iq_j}\rangle=\sqrt{1/2}d^{\alpha\beta\gamma}q_i^\beta q_j^\gamma\ , \tag{C3}$$

$$|\bar{6}^\alpha_{\bar{q}_i\bar{q}_j}\rangle=\sqrt{1/2}d^{\alpha\beta\gamma}\bar{q}_i^\beta\bar{q}_j^\gamma\ , \tag{C4}$$

where $\epsilon^{\alpha\beta\gamma}$ is the usual antisymmetric alternating symbol with $\epsilon^{123}=1$, $q_i^\alpha(\bar{q}_i^\alpha)$ represents the ith quark (antiquark) of color (anticolor) α, and the nonzero d's are

$$d^{111}=d^{322}=d^{633}=\sqrt{2}\ , \tag{C5}$$

$$d^{212}=d^{221}=d^{413}=d^{431}=d^{523}=d^{532}=1\ . \tag{C6}$$

The normalized color-singlet wave functions constructed from (C1) to (C6) are

$$|\bar{3}_{12}3_{34}\rangle=\sqrt{1/12}\epsilon^{\alpha\beta\gamma}\epsilon^{\alpha\rho\sigma}|q_1^\beta q_2^\gamma\bar{q}_3^\rho\bar{q}_4^\sigma\rangle\ , \tag{C7}$$

$$|6_{12}\bar{6}_{34}\rangle=\sqrt{1/12}d^{\alpha\beta\gamma}d^{\alpha\rho\sigma}|q_1^\beta q_2^\gamma\bar{q}_3^\rho\bar{q}_4^\sigma\rangle\ . \tag{C8}$$

It is clear that the constraints imposed by the symmetries of the Hamiltonian in the equal mass limit under $1\leftrightarrow2$ and $3\leftrightarrow4$ interchanges will be most easily implemented in the $\bar{\mathbf{3}}\mathbf{3}-\mathbf{6}\bar{\mathbf{6}}$ basis: the $\bar{\mathbf{3}}$ and **3** are antisymmetric under these interchanges while the **6** and $\bar{\mathbf{6}}$ are symmetric.

To transform to the mesonlike bases use

$$|1_{13}1_{24}\rangle=\sqrt{1/3}|\bar{3}_{12}3_{34}\rangle+\sqrt{2/3}|6_{12}\bar{6}_{34}\rangle\ , \tag{C9}$$

$$|8_{13}8_{24}\rangle=-\sqrt{2/3}|\bar{3}_{12}3_{34}\rangle+\sqrt{1/3}|6_{12}\bar{6}_{34}\rangle\ , \tag{C10}$$

and

$$|1_{14}1_{23}\rangle=\sqrt{1/9}|1_{13}1_{24}\rangle+\sqrt{8/9}|8_{13}8_{24}\rangle\ , \tag{C11}$$

$$|8_{14}8_{23}\rangle=\sqrt{8/9}|1_{13}1_{24}\rangle-\sqrt{1/9}|8_{13}8_{24}\rangle\ . \tag{C12}$$

From this last set of equations one can see that the states $|1_{13}1_{24}\rangle$ and $|1_{14}1_{23}\rangle$ span the space of internal color states; it is this observation that leads to the wave function based on (23)–(26) of the text.

Finally, we list the matrix elements of the color Casimir operator $\mathbf{F}_i\cdot\mathbf{F}_j$ in the $(|1_{13}1_{24}\rangle,|1_{14}1_{23}\rangle)$ basis:

$$\langle 1_{13}1_{24}|\begin{bmatrix}\mathbf{F}_1\cdot\mathbf{F}_2\\ \mathbf{F}_1\cdot\mathbf{F}_3\\ \mathbf{F}_1\cdot\mathbf{F}_4\\ \mathbf{F}_2\cdot\mathbf{F}_3\\ \mathbf{F}_2\cdot\mathbf{F}_4\\ \mathbf{F}_3\cdot\mathbf{F}_4\end{bmatrix}|1_{13}1_{24}\rangle=\begin{bmatrix}0\\ -\frac{4}{3}\\ 0\\ 0\\ -\frac{4}{3}\\ 0\end{bmatrix}\ , \tag{C13}$$

$$\langle 1_{14}1_{23}|\begin{bmatrix}\mathbf{F}_1\cdot\mathbf{F}_2\\ \mathbf{F}_1\cdot\mathbf{F}_3\\ \mathbf{F}_1\cdot\mathbf{F}_4\\ \mathbf{F}_2\cdot\mathbf{F}_3\\ \mathbf{F}_2\cdot\mathbf{F}_4\\ \mathbf{F}_3\cdot\mathbf{F}_4\end{bmatrix}|1_{14}1_{23}\rangle=\begin{bmatrix}0\\ 0\\ -\frac{4}{3}\\ -\frac{4}{3}\\ 0\\ 0\end{bmatrix}\ , \tag{C14}$$

$$\langle 1_{13}1_{24}|\begin{bmatrix}\mathbf{F}_1\cdot\mathbf{F}_2\\ \mathbf{F}_1\cdot\mathbf{F}_3\\ \mathbf{F}_1\cdot\mathbf{F}_4\\ \mathbf{F}_2\cdot\mathbf{F}_3\\ \mathbf{F}_2\cdot\mathbf{F}_4\\ \mathbf{F}_3\cdot\mathbf{F}_4\end{bmatrix}|1_{14}1_{23}\rangle=\begin{bmatrix}+\frac{4}{9}\\ -\frac{4}{9}\\ -\frac{4}{9}\\ -\frac{4}{9}\\ -\frac{4}{9}\\ +\frac{4}{9}\end{bmatrix}\ . \tag{C15}$$

APPENDIX D: SPIN WAVE FUNCTIONS AND MATRIX ELEMENTS

The calculations described in the text depend on spin wave functions and on transformations between various spin bases. In the qq and $\bar{q}\,\bar{q}$ spaces the scalar S and axial-vector $\mathbf{A}$ spin wave functions are

$$S_{ij}\equiv\sqrt{1/2}(\uparrow_i\downarrow_j-\downarrow_i\uparrow_j)\ , \tag{D1}$$

$$\mathbf{A}_{ij}\equiv(A_{ij}^{+},A_{ij}^{0},A_{ij}^{-})$$
$$=[\uparrow_i\uparrow_j,\sqrt{1/2}(\uparrow_i\downarrow_j+\downarrow_i\uparrow_j),\downarrow_i\downarrow_j]\ . \tag{D2}$$

The $qq\bar{q}\,\bar{q}$ spin states with total spin zero are

$$|S_{12}S_{34}\rangle=S_{12}S_{34}\ , \tag{D3}$$

$$|\mathbf{A}_{12}\cdot\mathbf{A}_{34}\rangle=\sqrt{1/3}(A_{12}^{+}A_{34}^{-}-A_{12}^{0}A_{34}^{0}+A_{12}^{-}A_{34}^{+})\ . \tag{D4}$$

To accomplish transformations to the meson bases we use the analogous spin states for pseudoscalar P_{ij} and vector mesons $\mathbf{V}_{ij}$:

$$|P_{13}P_{24}\rangle=\sqrt{1/4}|S_{12}S_{34}\rangle+\sqrt{3/4}|\mathbf{A}_{12}\cdot\mathbf{A}_{34}\rangle\ , \tag{D5}$$

$$|P_{14}P_{23}\rangle=-\sqrt{1/4}|S_{12}S_{34}\rangle+\sqrt{3/4}|\mathbf{A}_{12}\cdot\mathbf{A}_{34}\rangle\ , \tag{D6}$$

$$|\mathbf{V}_{13}\cdot\mathbf{V}_{24}\rangle=\sqrt{3/4}|S_{12}S_{34}\rangle-\sqrt{1/4}|\mathbf{A}_{12}\cdot\mathbf{A}_{34}\rangle\ , \tag{D7}$$

$$|\mathbf{V}_{14}\cdot\mathbf{V}_{23}\rangle=-\sqrt{3/4}|S_{12}S_{34}\rangle-\sqrt{1/4}|\mathbf{A}_{12}\cdot\mathbf{A}_{34}\rangle\ . \tag{D8}$$

The matrix element of $\mathbf{S}_i\cdot\mathbf{S}_j$ in the bases (D3) and (D4) are

$$\langle S_{12}S_{34}|\begin{bmatrix}\mathbf{S}_1\cdot\mathbf{S}_2\\ \mathbf{S}_1\cdot\mathbf{S}_3\\ \mathbf{S}_1\cdot\mathbf{S}_4\\ \mathbf{S}_2\cdot\mathbf{S}_3\\ \mathbf{S}_2\cdot\mathbf{S}_4\\ \mathbf{S}_3\cdot\mathbf{S}_4\end{bmatrix}|S_{12}S_{34}\rangle=\begin{bmatrix}-\frac{3}{4}\\ 0\\ 0\\ 0\\ 0\\ -\frac{3}{4}\end{bmatrix}\ , \tag{D9}$$

$$\langle\mathbf{A}_{12}\cdot\mathbf{A}_{34}|\begin{bmatrix}\mathbf{S}_1\cdot\mathbf{S}_2\\ \mathbf{S}_1\cdot\mathbf{S}_3\\ \mathbf{S}_1\cdot\mathbf{S}_4\\ \mathbf{S}_2\cdot\mathbf{S}_3\\ \mathbf{S}_2\cdot\mathbf{S}_4\\ \mathbf{S}_3\cdot\mathbf{S}_4\end{bmatrix}|\mathbf{A}_{12}\cdot\mathbf{A}_{34}\rangle=\begin{bmatrix}\frac{1}{4}\\ -\frac{1}{2}\\ -\frac{1}{2}\\ -\frac{1}{2}\\ -\frac{1}{2}\\ \frac{1}{4}\end{bmatrix}\ , \tag{D10}$$

$$\langle S_{12}S_{34}|\begin{bmatrix}\mathbf{S}_1\cdot\mathbf{S}_2\\ \mathbf{S}_1\cdot\mathbf{S}_3\\ \mathbf{S}_1\cdot\mathbf{S}_4\\ \mathbf{S}_2\cdot\mathbf{S}_3\\ \mathbf{S}_2\cdot\mathbf{S}_4\\ \mathbf{S}_3\cdot\mathbf{S}_4\end{bmatrix}|\mathbf{A}_{12}\cdot\mathbf{A}_{34}\rangle=\begin{bmatrix}0\\ -\sqrt{3}/4\\ \sqrt{3}/4\\ \sqrt{3}/4\\ -\sqrt{3}/4\\ 0\end{bmatrix}\ . \tag{D11}$$

APPENDIX E: A SIMPLIFIED ANALYSIS OF PRODUCTION PROCESSES

In the context of the coupled-channel equations of the text, the production of S-wave pseudoscalar-meson pairs can be studied via the addition of source terms. In the single-channel pointlike approximation one would write

$$-\frac{1}{2\mu}\nabla^2\psi(\mathbf{r})+V\psi(\mathbf{r})+\Sigma(\mathbf{r})=E\psi(\mathbf{r})\ , \tag{E1}$$

where $\Sigma(\mathbf{r})$ is some production source. [We can visualize $\Sigma(\mathbf{r})$ as being a cross-channel coupling $W(\mathbf{r})\psi'(\mathbf{r})$ in which we ignore the effect of the coupling on the primed channel.] Such an equation can, of course, only describe the production of pseudoscalar-meson pairs in the approximation in which their interaction with other particles participating in the reaction can be ignored.

If $V=0$, then Eq. (E1) can easily be solved by noting that

$$(\nabla^2+k^2)\frac{\cos(k|\mathbf{r}-\mathbf{r}'|)}{4\pi|\mathbf{r}-\mathbf{r}'|}=-\delta^3(\mathbf{r}-\mathbf{r}') \tag{E2}$$

so that, with $k=\sqrt{2\mu E}$, Eq. (E1) has the solution

$$\psi^{\text{free}}(\mathbf{r})=-\int d^3r'\frac{\cos(k|\mathbf{r}-\mathbf{r}'|)}{4\pi|\mathbf{r}-\mathbf{r}'|}2\mu\Sigma(\mathbf{r}') + \psi^{\text{free}}_{\Sigma=0}(\mathbf{r}) , \tag{E3}$$

where $\psi^{\text{free}}_{\Sigma=0}(\mathbf{r})$ is the most general solution of Eq. (E1) with $V=\Sigma=0$. If we simplify to a source at the origin,

$$\Sigma(\mathbf{r}')=\sigma\delta^3(\mathbf{r}') , \tag{E4}$$

then the most general free S-wave solution is

$$u_S^{\text{free}}(r)=-\frac{2\mu\sigma}{\sqrt{4\pi}}\cos(kr)+\alpha\sin(kr) \tag{E5}$$

which leads to a solution with outgoing waves of

$$u_S^{+\text{free}}(r)=-\frac{2\mu\sigma}{\sqrt{4\pi}}e^{ikr} \tag{E6}$$

as usual. Now consider the case that $V(\mathbf{r})$ is a square well of range a and depth $-V_0$. In this case the driven S-wave solution is

$$u_S(r)=-\frac{2\mu\sigma}{\sqrt{4\pi}}\times\begin{cases}\cos(k_0r), & r\le a ,\\ \sqrt{\cos^2(k_0a)+(k_0^2/k^2)\sin^2(k_0a)}\cos(kr+\eta), & r\ge a ,\end{cases} \tag{E7}$$

where $k_0=\sqrt{k^2+2\mu V_0}$ and $\tan(ka+\eta)=(k_0/k)\tan(k_0a)$. Since the solution of the $\Sigma=0$ equation is now that of Appendix B with $V\neq0$, the most general solution is

$$u_S(r)=\begin{cases}\dfrac{-2\mu\sigma}{\sqrt{4\pi}}\cos(k_0r)+\dfrac{\gamma(k/k_0)\sin(k_0r)}{\sqrt{\cos^2(k_0a)+(k^2/k_0^2)\sin^2(k_0a)}}, & r\le a ,\\ \dfrac{-2\mu\sigma}{\sqrt{4\pi}}\sqrt{\cos^2(k_0a)+(k_0^2/k^2)\sin^2(k_0a)}\cos(kr+\eta)+\gamma\sin(kr+\delta), & r\ge a ,\end{cases} \tag{E8}$$

leading to an outgoing wave solution

$$u_S^{+}(r)=-\frac{2\mu\sigma}{\sqrt{4\pi}}\times\begin{cases}\cos(k_0r)+ie^{i(\delta-\eta)}\left[\dfrac{k^2\cos^2(k_0a)+k_0^2\sin^2(k_0a)}{k_0^2\cos^2(k_0a)+k^2\sin^2(k_0a)}\right]^{1/2}\sin(k_0)r, & r\le a ,\\ \sqrt{d(k)}e^{i(kr+\delta)}, & r\ge a ,\end{cases} \tag{E9}$$

where

$$d(k)=\frac{k_0^2}{k_0^2\cos^2(k_0a)+k^2\sin^2(k_0a)} \tag{E10}$$

is the enhancement factor (B11) which appears in Eq. (39). Thus the production of this channel is enhanced by exactly the same "wave function at the origin" factor as a simple decay and it appears with the elastic phase δ as required by Watson's theorem.

In a multichannel problem the only essential complication is that there will, in general, be (complex) source terms $\sigma_1,\sigma_2,\ldots$ for each channel. This is true even if there is only one open channel. Thus the prediction of production amplitudes in general requires that one also predict the σ's. With a given dynamical model for the σ's, however, multichannel production is a straightforward generalization of the single-channel case.

[1]J. Weinstein and N. Isgur, Phys. Rev. Lett. **48**, 659 (1982); Phys. Rev. D **27**, 588 (1983).

[2]For disucssions of these problems, see, for example, A. J. G. Hey and D. Morgan, Rep. Prog. Phys. **41**, 675 (1978); A. D. Martin, in *Gauge Theories and Leptons,* proceedings of the 13th Rencontre de Moriond, Les Arcs, France, 1978, edited by J. Tran Thanh Van (Editions Frontières, Dreux, France, 1978), p. 363; D. Morgan, Phys. Lett. **51B**, 71 (1974).

[3]S. Godfrey and N. Isgur, Phys. Rev. D **32**, 189 (1985).

[4]R. Kokoski and N. Isgur, Phys. Rev. D **35**, 907 (1987).

[5]A. Le Yaouanc, L. Oliver, O. Péne, and J. C. Raynal, Phys. Rev. D **8**, 2223 (1973); **9**, 1415 (1974); **11**, 1272 (1975); M. Chaichian and R. Kogerler, Ann. Phys. (N.Y.) **124**, 61 (1980).

[6]F. E. Barnes, Phys. Lett. **165B**, 434 (1985); in *Photon-Photon Collisions,* proceedings of the Seventh International Workshop, Paris, France, 1986, edited by A. Courau and P. Kessler (World Scientific, Singapore, 1987), p. 25.

[7]See, e.g., Mark III Collaboration, Lutz Kopke, in *Proceedings of the XXIII International Conference on High Energy Physics,* Berkeley, California, 1986, edited by S. Loken (World Scientific, Singapore, 1987), p. 692.

[8]See, e.g., DM2 Collaboration, B. Jean-Marie, in *Proceedings of the XXIII International Conference on High Energy Physics* (Ref. 7), p. 689.

[9]R. L. Jaffe, Phys. Rev. D **15**, 267 (1977); **15**, 281 (1977); R. L. Jaffe and K. Johnson, Phys. Lett. **60B**, 201 (1976); R. L. Jaffe,

Phys. Rev. D **17**, 1444 (1978).

[10]We would not go so far, however, as to say that it is necessarily more appropriate than the P-matrix-supplemented bag model [R. L. Jaffe and F. E. Low, Phys. Rev. D **19**, 2105 (1979)], but it is difficult to push the P-matrix studies of these states far enough to allow a comparison with our results. See R. P. Bickerstaff, Philos. Trans. R. Soc. London **A309**, 611 (1983); Phys. Rev. D **27**, 1178 (1983). For a possible way to avoid some of the difficulties of the bag model for the S^* and δ, see N. N. Achasov, S. A. Devyanin, and G. N. Shestakov, Phys. Lett. **96B**, 168 (1980); Usp. Fiz. Nauk **142**, 361 (1984) [Sov. Phys. Usp. **27**, 161 (1984)].

[11]The $\mathbf{F}_i\cdot\mathbf{F}_j$ model has a venerable history, beginning with Y. Nambu, in *Preludes in Theoretical Physics,* edited by A. de Shalit, H. Feshbach, and L. van Hove (North-Holland, Amsterdam, 1966), p. 133. For the first discussions relevant to $qq\bar{q}\,\bar{q}$, see H. J. Lipkin, Phys. Lett. **45B**, 267 (1973); **58B**, 97 (1975); and in *Common Problems in Low- and Medium-Energy Nuclear Physics,* proceedings of the NATO Advanced Study Institute, Banff, 1978, edited by B. Castel, B. Gouland, and F. C. Khanna (Plenum, New York, 1978), p. 173. For a good review of $\mathbf{F}_i\cdot\mathbf{F}_j$ confinement, and especially a discussion of long-range van der Waals forces, see O. W. Greenberg and Harry J. Lipkin, Nucl. Phys. **A370**, 349 (1981), and references therein, including M. B. Gavela *et al.*, Phys. Lett. **82B**, 431 (1979); G. Feinberg and J. Sucher, Phys. Rev. D **20**, 1717 (1979). The relationship of these problems of the $\mathbf{F}_i\cdot\mathbf{F}_j$ model to its lack of local color gauge invariance is discussed in H. J. Lipkin, Phys. Lett. **113B**, 490 (1982); O. W. Greenberg and J. Hietarinta, *ibid.* **86B**, 309 (1979); Phys. Rev. D **22**, 993 (1980); D. Robson, *ibid.* **35**, 1018 (1987). The latter two sets of authors propose a solution to this problem which contains the essential features of the solution which emerges from the model of Ref. 12.

[12]N. Isgur and J. Paton, Phys. Rev. D **31**, 2910 (1985).

[13]N. Isgur and H. J. Lipkin, Phys. Lett. **99B**, 151 (1981); H. J. Lipkin, *ibid.* **124B**, 509 (1983).

[14]For early work on hybrid mesons see F. E. Barnes, Caltech Ph.D. thesis, 1977 (unpublished); Z. Phys. C **10**, 275 (1981); D. Horn and J. Mandula, Phys. Rev. D **17**, 898 (1978); P. Hasenfratz, R. R. Horgan, J. Kuti, and J. M. Richard, Phys. Lett. **95B**, 299 (1980); T. Barnes, F. E. Close, and F. de Viron, Nucl. Phys. **B224**, 241 (1983); T. Barnes and F. E. Close, Phys. Lett. **116B**, 365 (1982); M. Chanowitz and S. Sharpe, Nucl. Phys. **B222**, 211 (1983).

[15]N. Isgur, R. Kokoski, and J. Paton, Phys. Rev. Lett. **54**, 869 (1985).

[16]The glueball representation of ordinary $q\bar{q}$ annihilation is not completely accurate. Among other things, it fails to take into account the U(1) anomaly. It is, however, not misleading in this context.

[17]See, for example, N. Isgur, Phys. Rev. D **12**, 3770 (1975); **13**, 122 (1976).

[18]This "toy" problem and some of the difficulties associated with it are discussed in Ref. 1. For some earlier work on the problem see M. Gavela *et al.*, Phys. Lett. **79B**, 459 (1978); I. M. Barbour and D. K. Ponting, Nucl. Phys. **B149**, 534 (1979); C. S. Kalman, R. L. Hall, and S. K. Misra, Phys. Rev. D **22**, 1908 (1980); J. M. Richard, in *New Flavors and Hadron Spectroscopy,* proceedings of the XVI Rencontre de Moriond, Les Arcs, France, 1981, edited by J. Tran Thanh Van (Editions Frontières, Dreux, France, 1981), p. 331; K. F. Liu and C. Wong, Phys. Lett. **107B**, 391 (1981); R. Aaron and M. H. Friedman, Phys. Rev. D **25**, 1964 (1982); I. M. Barbour and D. K. Ponting, Z. Phys. C **5**, 221 (1980).

[19]Speculations about the $qq\bar{q}\,\bar{q}$ system date back to duality arguments: J. L. Rosner, Phys. Rev. Lett. **21**, 950 (1968); Phys. Rep. **11C**, 89 (1974); M. Fukugita and K. Igi, *ibid.* **31C**, 237 (1977); G. F. Chew, in *Proceedings of the Third European Symposium on $N\bar{N}$ Interactions,* Stockholm, Sweden, 1976, edited by G. Ekspong and S. Nilsson (Pergamon, New York, 1976), p. 515; V. A. Novikov *et al.*, Phys. Rep. **41C**, 1 (1978). The possibility of high angular momentum narrow baryonium is discussed in the potential model in Refs. 18, in the bag model, in A. T. Aerts, P. J. Mulders, and J. J. de Swart, Phys. Rev. D **21**, 1370 (1980); P. Hasenfratz and J. Kuti, Phys. Rep. **40C**, 75 (1978), and in string/Regge models, in Chan Hong Mo and H. Hogaasen, Phys. Lett. **72B**, 121 (1977); Nucl. Phys. **B136**, 401 (1978); Phys. Lett. **72B**, 400 (1977); **76B**, 634 (1978); M. I. Machi, S. Otsuki, and F. Toyoda, Prog. Theor. Phys. **57**, 517 (1977); X. Artru, Nucl. Phys. **B85**, 442 (1975); G. C. Rossi and G. Veneziano, *ibid.* **B123**, 507 (1977); G. F. Chew and C. Rosenzweig, Phys. Rep. **41C**, 263 (1978); A. W. Hendry and I. Hinchliffe, Phys. Rev. D **18**, 3453 (1978); W. W. Buck, C. B. Dover, and J. M. Richard, Ann. Phys. (N.Y.) **121**, 47 (1979), and references therein.

[20]C. W. Wong and K. F. Liu, Phys. Rev. D **21**, 2039 (1980).

[21]See, e.g., T. T. Chao and C. N. Yang, Phys. Rev. **170**, 1591 (1968).

[22]For a review of the history of scalar mesons, see L. Montanet, Rep. Prog. Phys. **46**, 337 (1983). For some very recent work and comprehensive references on the $I=0$ scalar channel, see K. L. Au, D. Morgan, and M. R. Pennington, Phys. Lett. **167B**, 229 (1986); Phys. Rev. D **35**, 1633 (1987).

[23]For $\pi\pi$ phase shifts we use the measurements of G. Grayer *et al.*, Nucl. Phys. **B75**, 189 (1974). For other measurements see A. A. Belkov *et al.*, Pis'ma Zh. Eksp. Teor. Fiz. **29**, 652 (1979) [JETP Lett. **29**, 597 (1979)]; L. Rosselet *et al.*, Phys. Rev. D **15**, 574 (1977); V. Srinivasan *et al.*, *ibid.* **12**, 681 (1975); N. M. Cason *et al.*, *ibid.* **28**, 1586 (1983).

[24]The data of Fig. 5 are a combination of the compilation of F. Wagner, in *Proceedings of the XVII International Conference on High Energy Physics,* London, England, 1974 (Rutherford Lab, Chilton, Didcot, England, 1974), p. II-27; (data with circles) and the data of W. Hoogland *et al.*, Nucl. Phys. **B126**, 109 (1977), which are the most recent of which we are aware (data with triangles). See also J. Prukop *et al.*, Phys. Rev. D **10**, 2055 (1974); D. Cohen *et al.*, *ibid.* **7**, 661 (1973); W. Hoogland *et al.*, Nucl. Phys. **B69**, 109 (1974).

[25]The Particle Data Group, G. P. Yost *et al.*, Phys. Lett. B **204**, 1 (1988).

[26]The experiment of D. Cohen *et al.*, Phys. Rev. D **22**, 2595 (1980), which is discussed in Ref. 27, is especially sensitive to the $\pi\pi\rightarrow K\bar{K}$ phase near $K\bar{K}$ threshold due to its exploitation of the tail of the $\rho(770)$.

[27]A. B. Wicklund *et al.*, Phys. Rev. Lett. **45**, 1469 (1980); A. B. Wicklund, in *New Flavors and Hadron Spectroscopy* (Ref. 18), p. 339.

[28]W. Wetzel *et al.*, Nucl. Phys. **B115**, 208 (1976); V. A. Polychronakos *et al.*, Phys. Rev. D **19**, 1317 (1979); G. Costa *et al.*, Nucl. Phys. **B175**, 402 (1980); A. Etkin *et al.*, Phys. Rev. D **28**, 1786 (1982).

[29]We are grateful to V. J. Pandharipande for emphasizing the possible importance of this coupling to us.

[30]J. Weinstein and N. Isgur (unpublished).

[31]N. Isgur, Nucl. Phys. **B243**, 189 (1984). This idea is an old one, see E. Fermi, *Elementary Particles* (Yale University Press, New Haven, CT, 1951), pp. 58–64.

[32]M. Frank, N. Isgur, P. J. O'Donnell, and J. Weinstein, Phys. Lett. **158B**, 443 (1985); Phys. Rev. D **32**, 2971 (1985).
[33]J. B. Gay *et al.*, Phys. Lett. **63B**, 220 (1976).
[34]D. Alde *et al.*, Nucl. Phys. **B269**, 485 (1986); Phys. Lett. B **198**, 286 (1987); **201**, 160 (1988), and references therein.
[35]N. A. Tornquist, Phys. Rev. Lett. **49**, 624 (1982).
[36]S. M. Flatté, Phys. Lett. **63B**, 224 (1976).
[37]F. E. Barnes, K. Dooley, and N. Isgur, Phys. Lett. B **183**, 210 (1987). There are several errors in this paper [see D. Morgan and M. R. Pennington, Z. Phys. C **37**, 431 (1988); **39**, 590(E) (1988)], but nothing wrong with the basic proposal that $I=0$ $\pi\pi$ threshold enhancements are to be expected.
[38]F. Feld-Dahme, Ludwig-Maximilians-Universität Ph.D. thesis, Munich, 1987.
[39]For examples of work on the vector-vector channels in the context of the bag model, see K. F. Liu and B. A. Li, Phys. Rev. Lett. **58**, 2288 (1987); **51**, 1510 (1983); Phys. Lett. **118B**, 435 (1982); **124B**, 550(E) (1983); Phys. Rev. D **30**, 630 (1984); N. N. Achasov, S. A. Devyanin, and G. N. Shestakov, Phys. Lett. **108B**, 134 (1982).
[40]H. J. Lipkin, Phys. Lett. **124B**, 509 (1983).